KU LEUVEN

FACULTY OF ENGINEERING TECHNOLOGY

CAMPUS GROUP T LEUVEN

Markerless Augmented Reality Guidance System for Maxillofacial Surgery

Ewald URY

Supervisor: Prof. Dr Ir Carlos Rodriguez
Co-supervisors: Ir Viktor Vörös
Prof. Dr Ir Emmanuel Vander Poorten
Dr Elke Van De Casteele
Dr Wouter De Vos

Master Thesis submitted to obtain the degree of Master of Science in Electromechanical Engineering Technology

Academic Year 2023 - 2024

©Copyright KU Leuven

Without written permission of the supervisor(s) and the author(s) it is forbidden to reproduce or adapt in any form or by any means any part of this publication. Requests for obtaining the right to reproduce or utilise parts of this publication should be addressed to KU Leuven, Campus GROUP T Leuven, Andreas Vesaliusstraat 13, 3000 Leuven, +32 16 30 10 30 or via e-mail fet.groupt@kuleuven.be

A written permission of the supervisor(s) is also required to use the methods, products, schematics and programs described in this work for industrial or commercial use, and for submitting this publication in scientific contests.

Acknowledgements

This thesis was fueled by curiosity and a beautiful collaboration between engineering and medicine. Through the exchange of ideas driven by our common interest in medical sciences, I would like to thank Dr Wouter De Vos for sharing his passion and trusting me with this project. A heartfelt acknowledgement to Elke Van De Casteele for her engineering advice, and to Dr Thibaut Buset for his medical insights.

To my promotor, Carlos Rodriguez, your enthusiasm for surgical technologies and scientific research has been both a guide and an inspiration. Thank you Viktor Vörös for your consistent guidance, kindness, and patience. Emmanuel Vander Poorten, for your inspiring ideas and for welcoming me into the Robot Assisted Surgery lab. Thank you, Marlon, Adlina, Giovanni and the rest of the lab for your help, as well as Mouloud and Priyanka for your precious input.

Clélia, thank you for being a source of motivation and strength throughout this journey. My thanks also to Harold and Douglas for your meticulous proofreading. To my family, roommates, and friends - your solidarity and willingness to listen to my daily adventures have been my steady support. And a special thanks to you, Lou, my dearest friend.

Abstract

Medical imaging, originating with X-rays in the late 19th century, has offered unparalleled insights into the body's inner workings. The advent of CT and MRI scanning revolutionised preoperative planning, allowing surgeons to perform intricate procedures with enhanced precision. However, a significant challenge remains in converting 2D images into 3D mental representations for accurate surgical navigation. In maxillofacial surgery, accurately transposing preoperatively planned osteotomies to the surgical environment is strenuous. The state-of-the-art cutting guide method proves to be cost- and time-consuming, with implications for the patient's health due to its invasive nature. Addressing this challenge, the proposed framework introduces an innovative markerless augmented reality spatial guidance system for maxillofacial surgery. This method replaces conventional physical cutting guides with virtual augmentations, simplifying the surgical workflow. To evaluate the proposed framework's usability and accuracy, an in-vitro user study involving four surgeons was conducted. The results showcased remarkable accuracy, with a hologram registration error of 1.08 mm. Suggestions for improvement included higher resolution of the holograms. An intra- and inter-operator hologram shift accuracy assessment revealed a mean registration error of less than 1.37 mm, underscoring the system's potential. These findings contribute significantly to ongoing advancements in the field of reconstructive surgery.

Keywords: Augmented reality, Markerless, Maxillofacial surgery, Microsoft HoloLens 2, Surgical navigation

Contents

Acknowledgements . . . . . **iii**

Abstract . . . . . **iv**

List of Figures . . . . . **vi**

List of Tables . . . . . **viii**

List of Symbols . . . . . **ix**

1 Introduction **1**

2 Background **3**

2.1 Maxillofacial reconstructive surgery and its challenges 3

2.2 Augmented reality in surgery 7

3 Materials & methods **18**

3.1 Development of the AR guidance system for mandible osteotomies 18

3.2 Experimental setup for accuracy measurement and user study 25

4 Results **31**

4.1 Accuracy of the registration 31

4.2 Cutting accuracy 33

5 Discussion **38**

5.1 Precision of the system 38

5.2 Scalability and future prospects 40

6 Conclusion **42**

Appendices **49**

A Python code for the EM sensor point cloud acquisition **A-1**

B NASA Task Load Index and questionnaire results **B-4**

List of Figures

2.1 Virtual preoperative planning of the osteotomies - from Materialise 3
2.2 Virtual preoperative planning of the cutting guides - from Materialise 4
2.3 Surgeons following the preoperative plan, guide screwing and opening of the leg . 5
2.4 Fibula's cutting guide and electric saw cutting 5
2.5 Reconstructed maxilla arch placement 6
2.6 Representation of current Extended Reality technologies 7
2.7 Comparison of Video See-Through and Optical See-Through devices 8
2.8 Overlay of virtual inferior alveolar nerve bundles 10
2.9 Surgical tool tracking using Augmented Reality Head-Mounted Displays 11
2.10 Marker tracking and pose estimation in pedicle screw placement 11
2.11 Demonstration of a virtual augmentation with Vuforia's Image Target 12
2.12 A markerless augmented reality image guidance method for dental implants 13
2.13 Fibula's cutting guide tracking using Vuforia's Model Target 14
2.14 A markerless registration method using a stereo camera and a 3D scanner 15
2.15 View of a virtual surgical plan overlayed on the face of a patient 16
2.16 Markerless registration method using the Iterative Closest Point algorithm 16
2.17 Markerless registration method using facial landmarks and machine learning . . . 17

3.1 Exploded view of the Microsoft HoloLens 2 19
3.2 3D model of the mandible derived from Computed Tomography Scans 20
3.3 Design of custom-made cutting guides in Blender 20
3.4 Overview of the main Vuforia Targets by categories 22
3.5 Overview of the Vuforia 10 Application Programming Interface 22
3.6 Process layout of the proposed markerless guidance system 23
3.7 Advanced View configuration in the Vuforia Model Target Generator application . . 24

3.8 Data flow between the Model Target Generator application and PTC servers 24
3.9 User's point of view of the proposed guidance system 25
3.10 Hologram accuracy assessment method 26
3.11 Intra-operator accuracy assessment setup 27
3.12 Two phases of the user study 28
3.13 Electromagnetic sensor data point acquisition 29
3.14 Distance between two points of the osteotomy lines 29

4.1 Hologram accuracy intra-operator assessment under surgical lighting conditions . . 32
4.2 The twelve mandibles and four cutting planes after the user study 33
4.3 Box plot of the user study accuracy across the different planes 35
4.4 Individual NASA Task Load Index results 36
4.5 Overall NASA Task Load Index results 36

List of Tables

4.1 Results of the inter-operator accuracy assessment 31

4.2 Results of the intra-operator accuracy assessment 32

4.3 Average initial registration time during the intra-operator accuracy assessment . . . 33

4.4 Results of the user study accuracy across the four surgeons 34

4.5 Results of the user study accuracy across the four planes 34

4.6 Time taken by the surgeons to draw the four osteotomy lines during the user study 37

List of Symbols

Symbols

δ	Mean error per pair of osteotomy lines
d_i	Euclidean distance between the i^{th} pair of points
σ	Standard deviation

Acronyms

AI	Artificial Intelligence
AR	Augmented Reality
CAD	Computer-Aided Design
CBCT	Cone Beam Computed Tomography
CT	Computed Tomography
EM	Electromagnetic
HMD	Head-Mounted Display
HPU	Holographic Processing Unit
ICP	Iterative Closest Point
IDE	Integrated Development Environment
IGVD	Image-Guided Visualisation Display
IMU	Inertial Measurement Unit
IR	Infrared
MRI	Magnetic Resonance Imaging
MTG	Model Target Generator
OR	Operating Room
OST	Optical See-Through
PCNL	Percutaneous Nephrolithotomy
PLA	Polylactic Acid
POV	Point of View
PNP	Perspective-n-Point
RAS	Robot Assisted Surgery
RM	Research Mode
RMSE	Root Mean Squared Error
SDK	Software Development Kit
SPECT	Single Photon Emission Computed Tomography
.STL	Standard Tessellation Language

TLX	Task Load Index
TOF	Time-of-Flight
UI	User Interface
UWP	Universal Windows Platform
UX	User Experience
UZA	Universitair Ziekenhuis Antwerpen
VSP	Virtual Surgical Planning
VST	Video See-Through

1 INTRODUCTION

In the ever-changing field of medical science and technology, real and virtual worlds have become increasingly connected. The combination of augmented reality (AR) and the complexity of surgical procedures has led the way to new ideas, innovation, and increasing precision in healthcare (Stucki et al., 2023). Maxillofacial reconstruction surgery, a field where dexterity and precision intersect, stands as evidence of this promising synergy.

Within the vast area of maxillofacial surgery, mandibular reconstruction is usually performed following trauma, tumour removal, or congenital abnormalities. Therefore, this procedure requires a high level of precision due to the vicinity of nerves and vessels (Patel et al., 2019). The state-of-the-art method for accurate execution of this operation first involves removing a part of the mandible, then transplanting segments of the fibula bone, along with its associated blood vessels and soft tissues, to recreate the ablated part of the mandible (Brown et al., 2017). The surgeon's cuts are typically guided by physical 3D-printed cutting guides, preoperatively designed to match the patient's unique anatomy (De Ketele et al., 2023). While yielding a precision of around 2 mm when compared to surgical planning (Pietruski et al., 2019), this method proved to be cost- and time-consuming, with implications for the patient's health due to its invasive nature. These challenges can be alleviated by replacing the physical cutting guides with virtual guidance, directly guiding the surgeon during the operation (Goormans et al., 2019).

Unlike virtual reality (VR), AR offers the opportunity to enhance the surgeon's view, while keeping close contact with the real world, providing real-time representation of the planned osteotomy trajectories (McCloskey et al., 2023). In the literature, preoperative data obtained from Computed Tomography (CT) Scans are segmented to reconstruct the desired anatomy, aiming to display this 3D information intraoperatively (Badiali et al., 2020). To precisely integrate the virtual content into the real scene, accurate real-time tracking of the environment needs to be implemented. Marker-based surgical tracking uses physical markers, placed on the surgical scene, as reference points to align or register the virtual content. As this requires some installation time, it primarily suffers from being invasive and limiting in the operating room (OR). On the other side, Markerless tracking aligns virtual and physical content without using physical markers, only relying on the patient's natural anatomical features or surface patterns. This makes it adaptable to changes in surgical conditions and eliminates the time and effort required to position the physical markers (Sadeghi-Niaraki and Choi, 2020).

Previous work at KU Leuven aimed to integrate AR guidance into maxillofacial surgery. However, the research did not achieve sufficient accuracy or real-time registration (Wybaillie, 2022). Building upon that, the goal of this thesis is to develop a markerless augmented reality guidance system for mandible reconstruction surgery. The aim is to replace the physical cutting guides with virtual cutting planes, directly guiding the surgeon's osteotomies through a custom application on a head-mounted display (HMD). As the ideal tracking system should work on its own (Casari et al., 2021), preferably with few additional hardware components and a well-designed user interface (UI), a

markerless tracking and registration approach was chosen. This aims to reduce operation time and cost, with less additional hardware in the OR, avoiding an overload of information. This thesis first provides a detailed description of a typical maxillofacial surgery, and the current state-of-the-art AR practises. The developed guidance system is then described and a method to assess the registration accuracy of the hologram on a phantom mandible is reported. To characterise the usability of the proposed framework, a user study involving four surgeons is performed in vitro.

To date, papers on AR-guided surgery primarily focused on marker-based tracking methods (Spirig et al. (2021); Martin-Gomez et al. (2022); Kavitha et al. (2023)). While these methods are precise, detecting and placing markers on the surgical field is invasive and time-consuming, requiring often invasive fiducial components. Other studies focused on markerless tracking techniques. These align virtual and real spaces without using physical markers, only relying on the patient's natural anatomical features or surface patterns. While promising, the current literature often uses cumbersome external hardware, such as hand-held displays (Kim et al., 2023), 3D scanners or external stereo cameras (Wang et al., 2019). Ceccariglia et al. (2022) proposed a markerless method to guide maxillofacial osteotomies with an HMD, comparing favourably with the state-of-the-art cutting guides method. However, lighting conditions and blood obstruction strongly affected the system. Furthermore, it only allowed the surgeon to approach the patient from one predefined angle.

This study contributes to the scientific literature in two distinct ways. Firstly, the system offers real-time markerless tracking of the patient's mandible, achieving a registration accuracy of less than 1.50 mm. Secondly, this system facilitates multi-angular tracking of the patient's mandible, thereby providing the surgeons with the flexibility to adjust their position comfortably throughout the surgical procedure.

2 BACKGROUND

2.1 Maxillofacial reconstructive surgery and its challenges

Before the surgery, the operating staff performs a detailed preoperative planning, that results in a step-by-step patient-specific approach. For this first phase, a clinical assessment of the patient's condition is carried out, including the evaluation of the cause and degree of the mandibular deformity. Medical imaging, such as CT scans and Magnetic Resonance Imaging (MRI), are performed to collect crucial patient-specific information. Virtual surgical planning (VSP) is conducted leveraging advanced technologies and is usually performed through a collaboration between surgeons and engineers (figure 2.1). These latter, usually working for a third-party company (e.g. Materialise, Leuven, Belgium), are responsible for designing and producing tailored-made cutting guides, which are meant to facilitate osteotomies[1], therefore playing a central role in this operation (Succo et al., 2014) (figure 2.2).

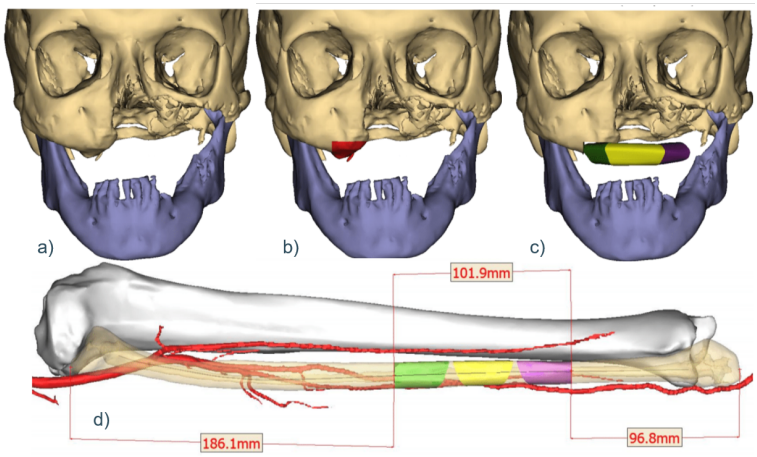


Figure 2.1: Virtual Surgical Planning of a real intervention seen in the University Hospital of Antwerp (UZA) - from Materialise ©. a) Preoperative scan of the patient's skull; b) maxilla area meant to be removed during the operation, indicated in red; c) arrangement of the three segments from the patient's fibula (in green, yellow and purple) to replace a portion of the patient's maxilla; d) lateral view of the corresponding three segments to be harvested from the fibula.

[1] Osteotomy: a surgical procedure that involves cutting bones (Cleveland, 2022)

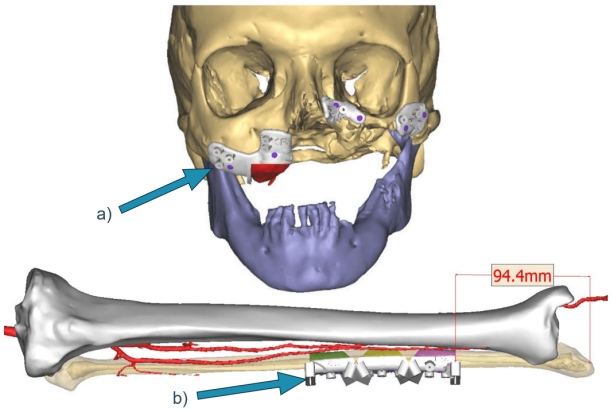


Figure 2.2: Virtual Surgical Planning of a real intervention seen in the UZA - from Materialise ©. a) Cutting guide mounted on the inferior part of the maxilla, for the mid-face resection, in red; b) anterior view of the cutting guide mounted on the fibula, with the three segments to be harvested.

Following the preoperative plan, the second phase of the intervention takes place in the OR. The patient is brought to the OR and prepared for anaesthesia, ensuring comfort and immobility throughout the intervention. A team of multiple surgeons will then cooperate with an anaesthetist, nurses and instrumentalists for more than 12 hours. First, the non-viable segment of the mandible is removed by the surgeons, while carefully following the preoperative planning as shown in figure 2.3, preserving vital vessels and tissues. The cutting guides, designed during preoperative planning, are screwed directly onto the patient's bone to guide precise osteotomies. To install the cutting guides firmly in place, soft tissues are scraped off the bone until the guides fit perfectly. After predrilling holes in the patient's bone, the guides are then screwed in place to allow precise osteotomies of the desired parts (figure 2.3, middle).

Then, the fibula harvesting process can start. After temporarily blocking blood circulation with a tourniquet, an incision is made along a longitudinal path marked by the surgeon. The latter then meticulously dissects through layers of skin, subcutaneous fat and fascia, ultimately exposing the fibula (figure 2.3, right). This process can last for a few hours, as attention is required here to preserve neurovascular canals.



Figure 2.3: Surgeons carefully following the preoperative plan (left); Screwing of the cutting guide onto the desired area (middle); Opening of the patient's leg to reach the fibula (right). The pictures were taken by the author during an intervention at the UZA.

Once the fibula is freed from any muscle or other tissue, the fibula cutting guide can finally be screwed securely into the bone, while trying to avoid damage to the surrounding nerves and vessels (figure 2.4, left). The fibula osteotomy is then performed using an oscillating saw, cutting the desired bone segments (figure 2.4, right).

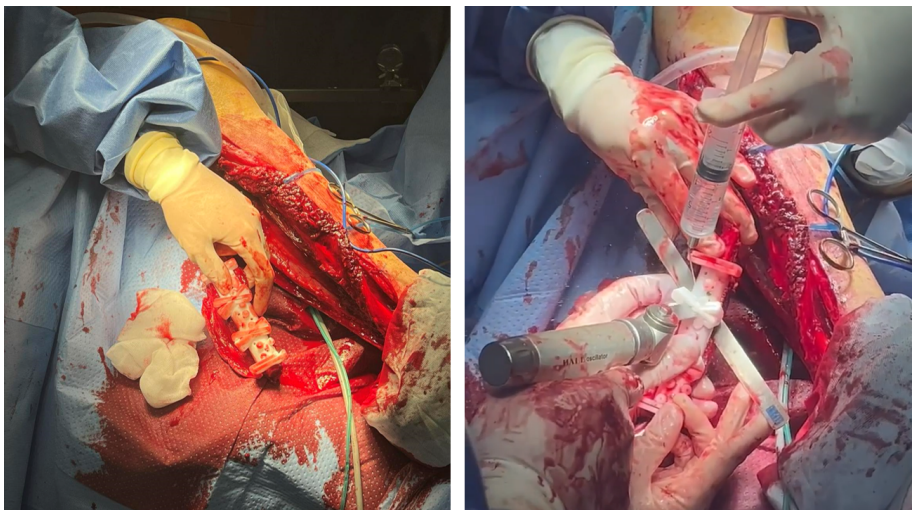


Figure 2.4: Fibula's cutting guide placed onto the patient's exposed fibula bone (left); Cutting of the fibula segments through the cutting guide, with a surgical electric saw (right). The pictures were taken by the author during an intervention at the UZA.

The third phase involves reconstructing the patient's face (here, the maxilla arch) with the fibula's segments (figure 2.5, left). The latter are assembled and securely fixed in place using bio-compatible titanium plates and screws, providing stability and support for the patient throughout the healing process (figure 2.5, middle).

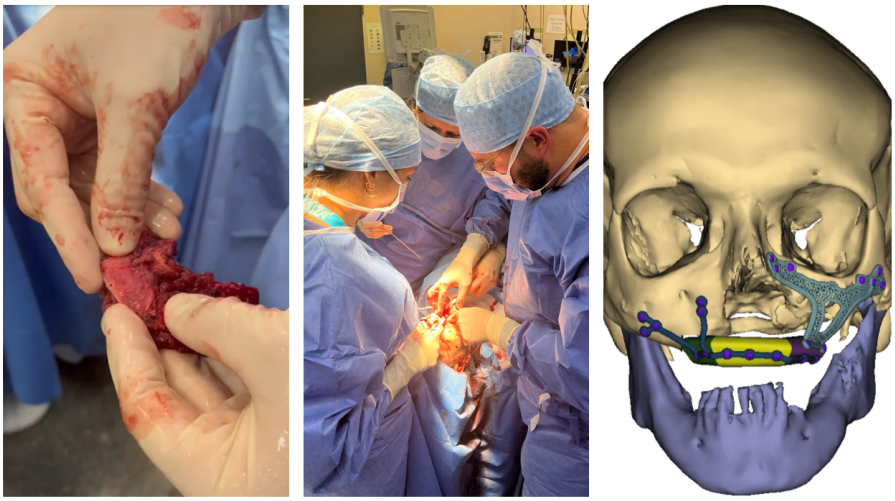


Figure 2.5: Reconstructed maxilla arch from the three fibula segments (left); Placement of the reconstructed arch in the patient's mouth (middle); final result with 3D-printed titanium implants (right). The first two pictures were taken by the author during an intervention at the UZA. The image on the right is from Materialise ©.

Finally, vascular anastomosis[2] is performed with great precision to re-establish blood supply to the graft. The soft tissues are then sutured, ensuring proper coverage of the resulting graft and allowing smooth wound healing. After more than 12 hours of operation, the patient is now reconstructed (figure 2.5, right) and can begin the healing process. The latter includes a postoperative rehabilitation program, focusing on functional aspects such as mastication, speech and walking exercises. Follow-up appointments are scheduled to monitor the reconstruction's long-term success (Wijbenga et al., 2016).

2.1.1 Challenges of the cutting guides

The Cutting Guide method has been proven to be a valuable advancement in mandibular reconstruction surgery. Through patient-specific design of the guides, precise and optimal cuts of the bones are ensured leading to fewer errors, and ultimately quicker patient recovery (Dong et al., 2017). Two studies compared postoperative medical images of osteotomies with their surgical plans. The first study compared postoperative CT scans with simulated osteotomies on 18 fibula models and found a mean deviation of 2.60 mm from their VSP (Pietruski et al., 2019). The second study analysed data from 26 patients who underwent mandibular reconstruction using a microvascular free fibula flap between January 2015 and June 2018. The study involved creating postoperative mandible models from CT scans and comparing these with preoperative plans. A mean deviation of 1.74 mm was found (Goormans et al., 2019).

However, this method is not without problems and limitations. Cutting guides are bulky and obstructing, preventing the surgeon from seeing blood vessels and nerves in real time, which can lead to dramatic consequences. Hard to accurately position, they need to be placed on the patient's bone before the surgeon can perform the osteotomy accurately (see figure 2.4). Furthermore, in addition

[2] vascular anastomosis means surgically reconnecting two blood vessels together (MedlinePlus, 2020)

to causing deterioration of the periosteum, placing the cutting guides is time-consuming and leads to longer ischaemia time[3], putting the patient's health at risk. Finally, designing and producing the 3D cutting guide pieces is expensive (Tarsitano et al., 2014) and requires the experience of a third-party company (e.g. Materialise ©, in Leuven). Pieces of plastic are also likely to fly into the patient's body when performing the osteotomies, leading to possible rejection by the patient's immune system (Battaglia et al., 2019).

2.2 Augmented reality in surgery

The integration of virtual reality, augmented reality and mixed reality (MR) into the medical field has opened new perspectives in surgical procedures. These technologies, originating from gaming and entertainment, have found applications in healthcare, enhancing the efficiency and precision of medical interventions (Verhey et al., 2020).

AR, in particular, has strongly emerged in the surgical landscape. Unlike VR, which completely immerses the user in a virtual environment, AR displays digital information in the real world, allowing surgeons to interact with both simultaneously (Ke et al., 2019). For example, this might mean projecting 3D images of the patient's anatomy onto the patient's body. This aims to not replace but rather enhance the surgeon's view of the real world. VR, on the other side, differs in that it fully immerses the user in a virtual environment. In surgery, VR is rather used for training and preoperative planning. Surgeons enter a virtual representation of the surgical field, allowing them to rehearse complex procedures in a risk-free environment before the operation (Pham Dang et al., 2021). Postoperatively, VR can also be therapeutic, and used in patient rehabilitation and pain management. MR, a combination of both AR and VR, further refines this interactive experience by allowing real-time manipulation of both physical and virtual environments (see figure 2.6) (McCloskey et al., 2023).

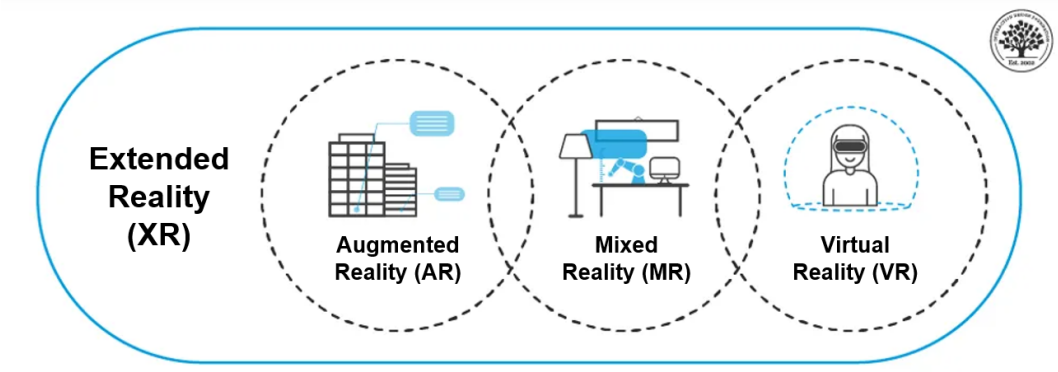


Figure 2.6: Representation of current extended reality (XR) technologies (Tremosa, 2023).

These immersive technologies collectively open new frontiers in preoperative planning, intraoperative guidance, and postoperative evaluation, significantly impacting patient outcomes and surgical accuracy. In particular, AR aims to enhance surgical precision by providing surgeons with real-time,

[3]The ischaemia time refers to the duration during which an organ or tissue is deprived of an adequate blood supply

augmented views, ultimately reducing the likelihood of errors. With more accurate guidance, the risk of damaging critical structures is significantly reduced, thereby ensuring greater patient safety and lower complication rates. AR-guided procedures often result in shorter operative times leading to better efficiency (Mai et al., 2023).

In AR, to provide a highly immersive experience for the user, HMDs can be used. HMDs are devices that provide a direct visual overlay of the virtual data onto the user's real-world view (Incekara et al., 2018). They are particularly useful in AR as they allow the users to see the relevant information within their field of view. Two categories can be distinguished: First, Video See-Through (VST) HMDs use external cameras to capture the real world and visualise it on displays placed in front of the user's eyes. The virtual content is rendered with the camera views, and the resultant video is then shown on the display, be it an external or a head-mounted display (see figure 2.7). This allows for precise control over what the user sees, including adjusting brightness, contrast, and other visual elements. This can be particularly advantageous in environments where lighting conditions are not ideal for AR experiences. The latter characteristic provides a distinct advantage over the other HMD technology, Optical See-Through (OST) devices, where an accurate registration between virtual and real-life objects can be challenging. OST devices project a holographic image on a transparent glass, allowing the user to still see the environment through the display. The visual quality, resolution, brightness, and colour accuracy, are usually higher compared to the camera-based view in VST HMDs. This can be crucial for applications where visual detail and colour fidelity are important. Furthermore, OST HMDs generally consume less power as they do not require cameras to capture the environment or powerful processors to render complex scenes (Badiali et al., 2020). HMDs could lead to time-saving decisions and a safer, more efficient workflow in surgical environment (Eckardt and Paulo, 2016). One of the most used HMDs in the context of augmented reality surgery is the Microsoft HoloLens 2 (Microsoft, Redmond, WA), an OST HMD with growing use in the OR that stands as one of the main references for AR-oriented surgery applications (Chegini et al., 2023).

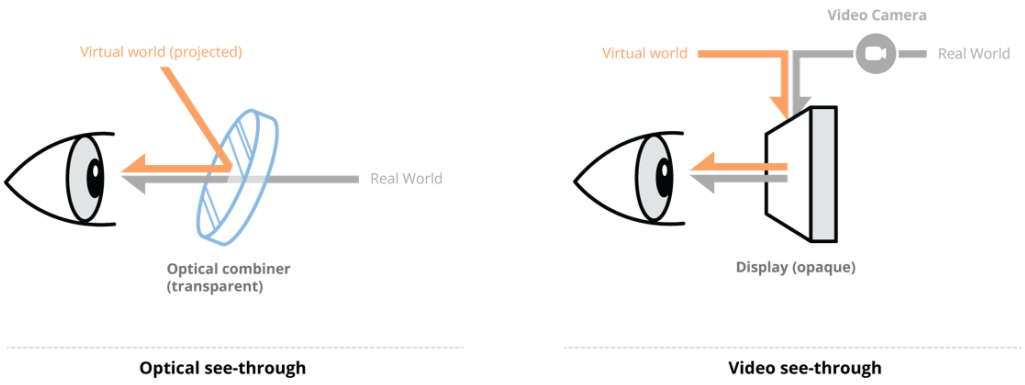


Figure 2.7: Comparison of Video See-Through and Optical See-Through devices. OST allows users to see the real world directly through transparent displays with digital augmentations superimposed (left), while VST allows the user to view the real world through a camera feed overlaid with digital imagery (right) (Yadav, 2018).

2.2.1 Existing AR practices in maxillofacial surgery and other surgical procedures

To visualise further contextual information in the form of AR guidance for maxillofacial surgery, a detailed medical imaging of the patient needs to be made. These preoperative modalities are segmented to reconstruct the patient's anatomy. 70% of cases used CT Scans or Cone Beam CT (CBCT) Scans (Badiali et al., 2020). For more complicated cases that involve tumour removal, multi-modal imaging is used, involving either a combination of MRI and CT Scans or Single Photon Emission Computed Tomography (SPECT) combined with CT Scans. Another method to obtain the patient's teeth shape is to use a 3D scanner together with CT imaging (Wang et al. (2019) and Ahn et al. (2019)). Image segmentation software is commonly used for processing raw data obtained from medical imaging, facilitating future virtual content creation.

Following the acquisition of medical imaging, the reconstructed anatomy is used to develop AR guidance for the surgery. Different types of virtual content can be displayed in the real scene to aid surgeons with their tasks, from preoperative planning to the final stages of the operation. A virtual mesh representation of anatomical features, from bony structures (mandible, maxilla, etc.) to tissues or soft structures (lymph nodes, tooth roots, nerve channels, arteries...) is typically used (Mischkowski et al. (2006), Suenaga et al. (2015), Scolozzi and Bijlenga (2017) and Wang et al. (2019)). This additional virtual content is usually added to the scene to aid with the precision or ease of the surgical procedure. For example, Zinser et al. (2013) used an interactive image-guided visualisation display (IGVD) to accurately show virtual maxillary positioning planning. Zhu et al. (2017) proposed a method to precisely guide the surgeon, showing virtual osteotomy planes, and inferior and alveolar nerve bundles during the operation (see figure 2.8). Their system integrates a noninvasive registration strategy using an occlusal splint with a fiducial marker, allowing for accurate superimposition of virtual images onto the real surgical environment, through a semi-transparent glass. The study involved 20 patients and demonstrated the AR system's high accuracy and practical feasibility in clinical settings, providing enhanced visualisation and improved surgical outcomes in maxillofacial surgeries. Although the occlusal splint caused some installation difficulties, the system's accuracy, easy manipulation, and cost-effectiveness are highlighted as significant benefits for surgical applications.

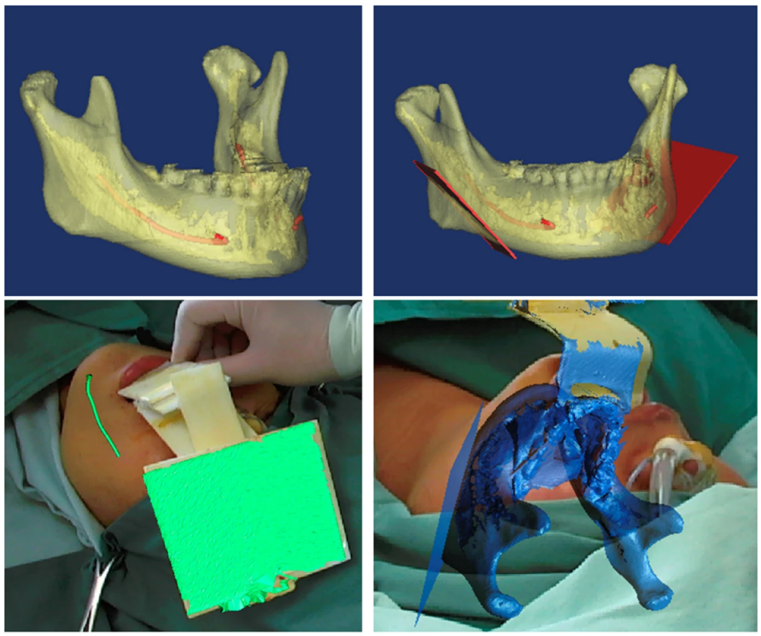


Figure 2.8: Overview of an image registration procedure using a custom-made occlusal splint for overlaying virtual inferior alveolar nerve bundles (Zhu et al., 2017).

Tracking method and registration: marker-based vs markerless approach

Accurate rendering of the AR content at its expected location is crucial for evaluating the precision, efficiency, and reliability of a particular surgical navigation system. To precisely integrate the virtual content into the real scene, the accurate real-time tracking of the environment constitutes the central objective of the implemented technique. There are various existing tracking methods, that can be divided into two categories: a marker-based approach, where physical fiducial components are tracked by the system's cameras, and a markerless approach, where the tracking relies on sensor or computer vision technologies to detect and track objects, without the need for physical markers (Sadeghi-Niaraki and Choi (2020)).

In marker-based tracking, physical markers are placed on the patient's body or a specific anatomical region. These markers are then scanned and used as reference points to align or register the virtual images (e.g. preoperative planning data or anatomical structures) with the actual physical space of the patient. This alignment ensures that the virtual data accurately corresponds to the patient's actual anatomy, aiding in precise navigation during surgical procedures. As proof of its high accuracy and reliability, Martin-Gomez et al. (2022) proposed a framework (see figure 2.9) that uses the built-in cameras of the Microsoft HoloLens 2 to accurately track the position and orientation of surgical tools through small spherical retro-reflective markers. They achieved an accuracy of 0.09 $\pm$ 0.06 mm on lateral translation and 0.42 $\pm$ 0.32 mm on longitudinal translation. Using a similar Infrared (IR) tracking approach in combination with the HoloLens, another paper obtained a registration accuracy of 0.76 mm. The authors noticed that, while the marker-based methods turn out to be precise, detecting and placing markers on the surgical field is invasive and time-consuming. Furthermore, any change in the surgical plan or the patient's position may require re-scanning or repositioning of the markers, leading to possible inaccuracies in registration (Kunz et al., 2020).

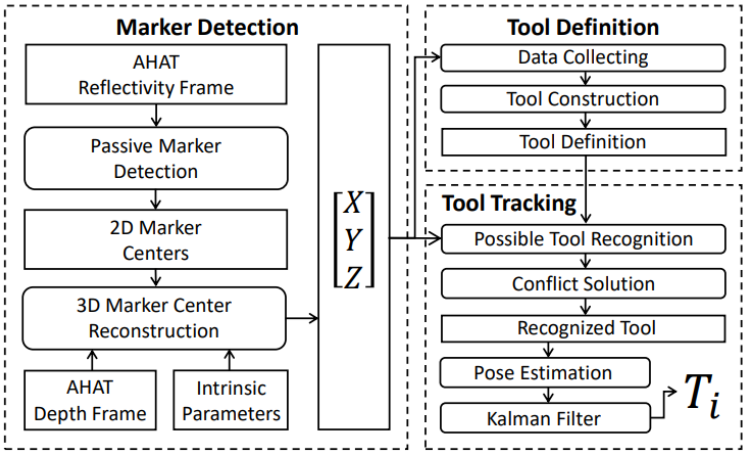


Figure 2.9: Overview of a framework for tracking surgical tools using the built-in cameras of AR HMDs. The process involves three steps: 1) Extracting the three-dimensional positions of retro-reflective markers observed by the AHAT camera; 2) Grouping these detected markers into subsets that match specific tool arrangements; 3) Determining the orientation and location ('pose') of these identified tools using the markers' positions in subsequent image frames (Martin-Gomez et al., 2022).

In other marker-based approaches, Liebmann et al. (2019) and Spirig et al. (2021) used fiducial markers (provided by AprilTags) for tracking using the cameras of the HoloLens that are accessible via its Research Mode (RM) functionality. The process involves intraoperative manual surface digitisation and holographic navigation, aiming for high precision in placing pedicle screws (see figure 2.10). An iterative closest point (ICP) algorithm was used to refine the registration of the virtual model on its physical counterpart. The algorithm iteratively adjusts the transformation (position and orientation) of the two objects (virtual and physical) to minimise the distance between corresponding points. It continues until a specified number of iterations is reached or the change in root mean squared error (RMSE) between two steps is below a certain threshold. The version with the smallest RMSE is then selected, ensuring the best possible alignment. They respectively achieved a registration accuracy of 2.77 mm and 4.74 mm.



Figure 2.10: Marker tracking and pose estimation in pedicle screw placement. a) Marker-based pointing instrument; b) in the experimental setup, a surgeon wears the HoloLens and uses the pointing instrument; c) the augmented view as seen by the surgeon while sampling the surface; d) vertebra L1 is overlaid post-registration (with the insertion points highlighted in blue) (Liebmann et al., 2019).

Condino et al. (2018) used the Vuforia Software Development Kit (SDK), more specifically their Image Target feature, to detect and track an image at runtime for orthopaedic surgery. It focuses on hip arthroplasty and aims to incorporate patient-specific anatomical models derived from CT scans. Once the image target marker is detected, Vuforia Engine starts tracking, and the system renders the virtual anatomy as long as the target is visible by the HoloLens 2 cameras. They found that fundamental attributes for precise Image Target tracking include good image contrast, no repetitive patterns and many details. An accuracy of 0.70 mm was found. Lee et al. (2018) detailed the process of creating a 3D model of the thyroid and surrounding structures from a patient's medical imaging files using segmentation software. The AR app, developed using Unity and Vuforia SDK, helps visualise internal organs on a medical training mannequin (see figure 2.11). The aim is to enhance surgical precision by localising critical tissues or organs that are difficult to view during surgery. This method holds the potential for extensive medical applications, offering a new dimension in surgical education and planning. Kavitha et al. (2023) used Vuforia's Image Target feature to detect and track IR markers. Frantz et al. (2018) experimented with Vuforia's Cylinder Target and obtained a perceived mean hologram drift of 1.41 mm.

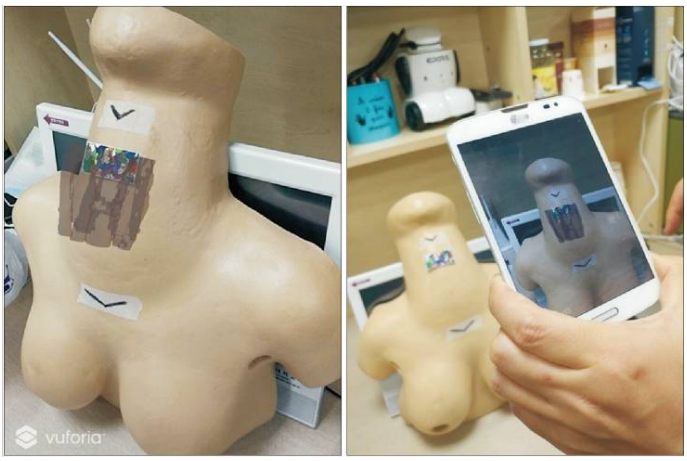


Figure 2.11: Demonstration of AR technology with Vuforia's Image Target tool, showcasing the thyroid and internal organs, rendered on a mannequin thyroidectomy training model, visualised through a smartphone (Lee et al., 2018).

While marker-based surgical navigation systems primarily suffer from being invasive and limiting in the OR, markerless tracking techniques align virtual and physical spaces without using physical markers, only relying on the patient's natural anatomical features or surface patterns. This makes it more adaptable to changes in surgical conditions and eliminates the time and effort required to position the physical markers. However, it has the drawback of being potentially less accurate than marker-based techniques, due to the added complexity of the tracking algorithms, not relying on fiducial markers anymore.

An article by Dong et al. (2023) addressed the limitations of traditional AR dental implant surgery navigation systems, which typically rely on markers. These markers often complicate the dentist's operations and cause discomfort to patients. To overcome these issues, the paper introduces a markerless image guidance method. This process begins with matching the image contours to define the connection between the current frame and a previously loaded initial frame. Following this, the camera's position is found by resolving the Perspective-n-Point (PnP) problem, to determine the

pose of the camera (its position and orientation) in a 3D space, given a set of 3D points in the world and their matching 2D projections on the camera's image plane (see figure 2.12). The registration error was found to be 0.73 $\pm$ 0.14 mm. The errors in the placement of dental implants were measured at various points: 1.17 $\pm$ 0.24 mm at the neck of the implant, 1.43 $\pm$ 0.39 mm at the apex, and an angular error of 5.57 $\pm$ 2.10°. These errors fall within acceptable clinical margins, indicating the method's efficacy. While the authors would include an algorithm to optimise illumination issues in future studies, the maximum error and its standard deviation were found to be within clinically acceptable ranges, underscoring the precision of this markerless AR method.

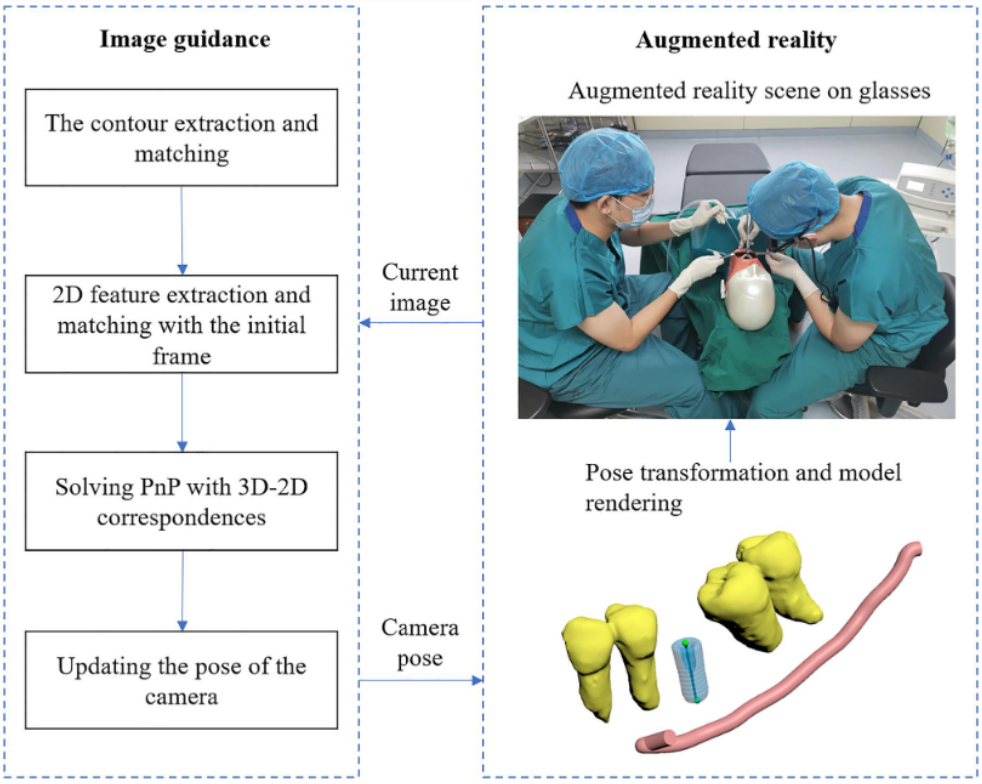


Figure 2.12: Overview of a markerless augmented reality image guidance method for dental implants. Once initialisation through contour matching is completed, the relationship between the current and preloaded initial frames is established by aligning their feature points. The camera's position and orientation are then determined by solving the PnP problem. The AR scene is then displayed on HiAR G200 optical glasses (Hiscene Information Technology, China) (Dong et al., 2023).

Gauthier Wybaillie, a former KU Leuven Biomedical Engineering student, wrote an innovative master's thesis focused on exploring the integration of AR in maxillofacial surgery. Specifically focusing on mandibular reconstruction with free fibular flap, it explored the development of a real-time tracking algorithm using ICP and point clouds generated from Hololens 2 sensors, with an emphasis on accuracy and real-time capabilities. The research identified challenges in achieving sufficient accuracy and real-time registration for practical surgical use (Wybaillie, 2022).

Through the use of Microsoft HoloLens 2, Piramide et al. (2022) proposed a markerless method to assist the pose of a virtual fibula cutting guide over its physical counterpart, to aid surgeons in mandibular reconstruction procedures. The application tracks the real cutting guide and computes

its distance from the final position, overlaying holograms in the surgeon's field of view (see figure 2.13). This was done using the "Model Target" feature by Vuforia. This tool enables the recognition and tracking of objects in the real world, making it possible to overlay virtual content on physical objects in the OR. Testing with volunteers showed an accuracy of 6 mm and the application's user-friendly interface, despite some initial learning difficulties. The authors reported a sensitivity of the Vuforia algorithm to variations in light.



(a) (b)

Figure 2.13: Example of fibula's cutting guide tracking using Vuforia's Model Target. a) The system displays a virtual model of the fibula in white, perfectly aligned with the actual bone and the prepositioned surgical guide during the procedure; b) additionally, as the real surgical guide is positioned, the system actively tracks and provides feedback on its placement through a virtual interface, indicating any deviations in both position and rotation from the predetermined correct location (Piramide et al., 2022).

Another study presented a novel markerless image registration method for maxillofacial surgery. They used a custom-made stereo camera system and an intraoral 3D scanner for acquiring the patient's teeth shape, improving surgical visualisation and accuracy (see figure 2.14). This method addresses challenges in AR surgical navigation, offering non-invasive, practical solutions without external fiducial markers, and allows real-time updates to counteract patient movement. While still relying on external hardware (with the stereo camera and 3D scanner), its effectiveness is demonstrated through jaw phantom experiments and yielded an accuracy of less than 0.50 mm, showcasing its potential to enhance surgical outcomes in oral and maxillofacial surgery (Wang et al., 2019).

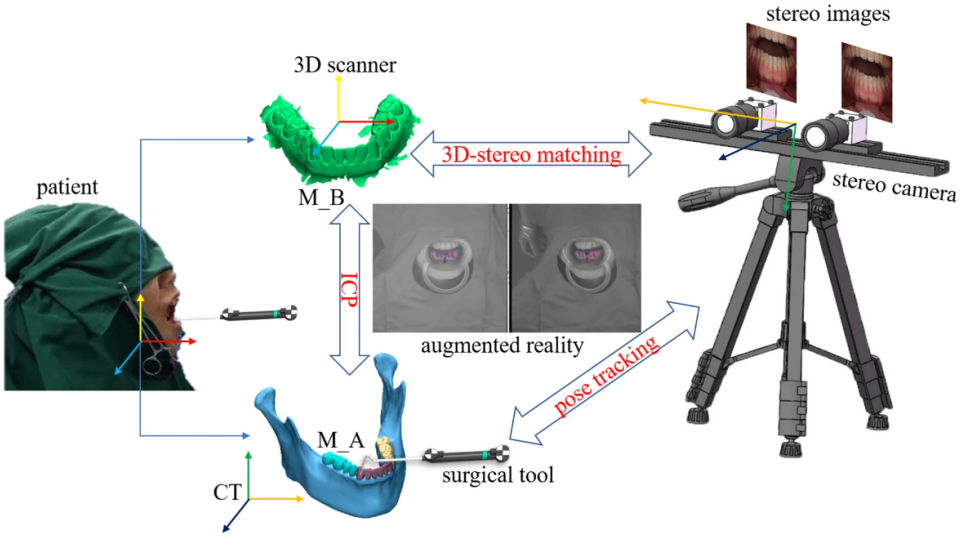


Figure 2.14: Overview of an image registration procedure. A custom-made stereo camera is placed to track the patient's teeth (Wang et al., 2019).

Cercenelli et al. (Cercenelli et al. (2022) and Ceccariglia et al. (2022)) aimed to evaluate the practicability of performing maxillary osteotomies using AR. The Model Target feature from Vuforia Engine was used along with the Microsoft HoloLens 2. One of the papers presents a markerless AR guidance system using the HoloLens, applied in surgeries for maxilla and mandible demolition. The study involved three cases of mandibular and maxillary oncologic resections. The AR system uses the Model Target method based on facial profile recognition (see figure 2.15). The results demonstrated the feasibility and viability of performing osteotomies under AR guidance, comparing favourably with the state-of-the-art cutting guides method. While described as a promising method, yielding an accuracy under 2 mm for both studies, the authors reported certain challenges. First, this markerless tracking method seems to be strongly affected by lighting conditions, ultimately affecting the registration performances. The used method is limited, as it only allows the surgeon to approach the maxilla from one predefined angle. On another note, tracking deformable or blood-obstructed anatomy remains a challenge. Finally, the users were mostly happy with the HoloLens 2 but noticed a low hologram render contrast, as well as some discomfort after wearing the HMD for a long period.



Figure 2.15: Surgeon's view of a surgical plan overlayed on the face of the patient. a) Virtual registration of the patient's skull and tumour obtained from CT Scans, and osteotomy planes obtained from preoperative planning; b) same view, without the skull (Ceccariglia et al., 2022).

Another study presented an innovative, automatic markerless method for bone registration and tracking in orthopaedic surgery. Utilising depth imaging and deep learning, the method captures bone images intraoperatively with a depth camera. Deep neural networks identify surgical targets and segment images to match the bone's surface with a preoperative model (see figure 2.16). This markerless approach, using a point-to-plane ICP algorithm shows a promising accuracy of 2.74 mm and high efficiency in ex vivo tests, aiming to enhance surgical workflow while reducing invasiveness and duration of procedures (Liu and Baena, 2020).

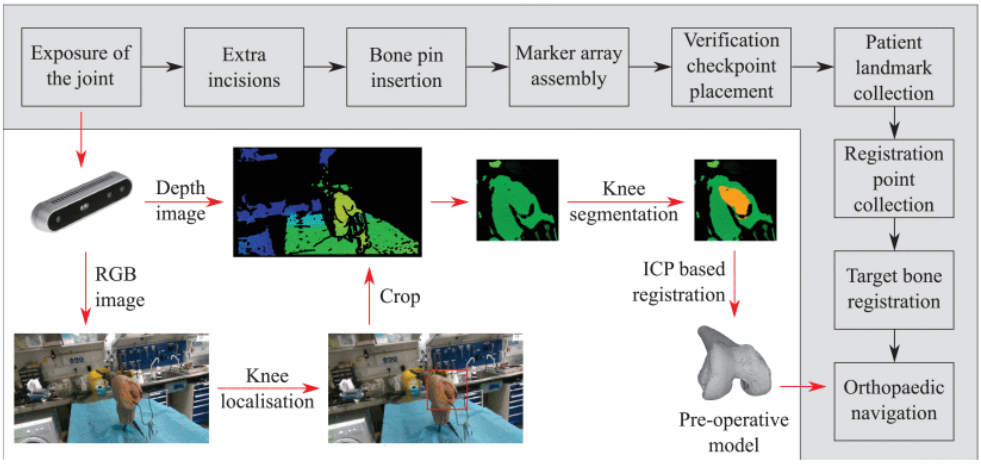


Figure 2.16: This image compares an automatic markerless registration with traditional orthopaedic registration methods. It shows the markerless registration workflow, shown in white, which works without the need for human intervention or physical markers. In contrast, in grey, is the conventional registration process used in orthopaedic navigation, involving more traditional, surgeon-dependent techniques.(Liu and Baena, 2020).

A study conducted by Pepe et al. (2019) focused on a novel method for integrating MR in maxillofacial surgery. It introduced a markerless registration system using CT scan information and the Microsoft HoloLens. The approach leverages facial landmark detection through Dlib (a toolkit

combining computer vision and machine learning for image processing (Trotta et al., 2019)) and the Spatial-Mapping API from Microsoft, for accurate alignment of virtual facial anatomy. The study includes a comparison with marker-based methods and gathers expert feedback, demonstrating the potential of this technology in surgical applications and its positive reception by medical professionals.

Kim et al. (2023) proposed a novel markerless AR system to enhance maxillofacial surgery precision. They used machine learning for registration, aligning CT scan data with 3D camera-captured point clouds. The study involved 20 patients, in a two-stage registration process as shown in figure 2.17: preliminary landmark detection and precise ICP algorithm alignment. The system's effectiveness was evaluated by measuring registration errors in various facial regions, both in awake and intubated patient states. Results showed a mean registration error of 1.49 $\pm$ 0.38 mm (awake) and 1.95 $\pm$ 0.64 mm (intubated), with increased errors in the lower face due to intubation. While this study visualised the AR content through a tablet device, requiring the surgeon's hands to be occupied, the findings demonstrate the system's potential in accurately visualising the facial region for surgical applications, highlighting its significance in improving facial plastic and reconstructive surgery outcomes.

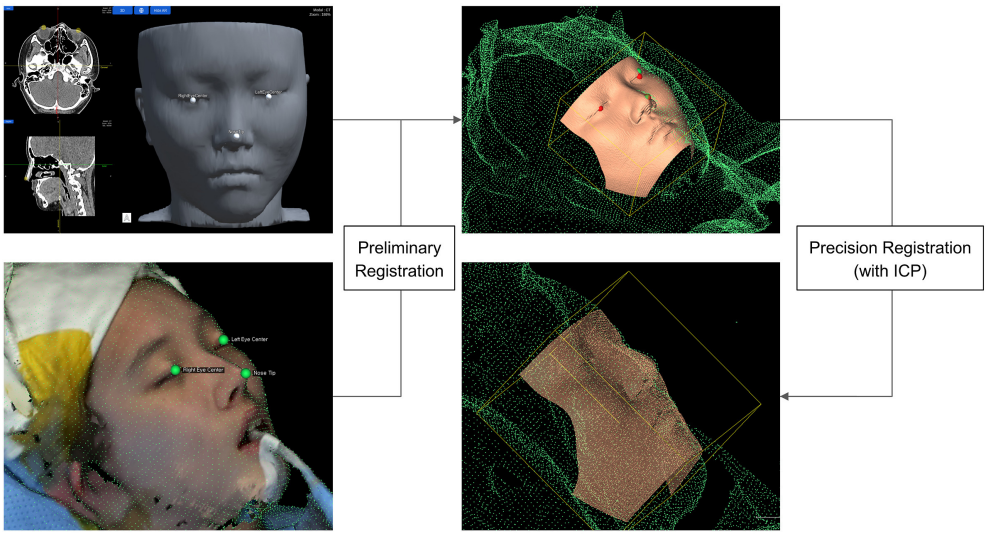


Figure 2.17: An AR registration method conducted sequentially. First, the Mediapipe framework was employed to acquire facial landmarks on a 3D height map. Subsequently, an initial registration stage was undertaken, where the CT model was approximately aligned with the 3D-photographic model. This step ensured reduced computation time and enhanced the accuracy of the following registration stage. The final phase involved precise registration, achieved by repeatedly applying the ICP algorithm a hundred times (Kim et al., 2023).

As a general remark, Casari et al. (2021) stated that, according to their literature review on AR in surgical applications, the ideal tracking system should work on its own, preferably with few additional hardware components and a well-designed UI, avoiding an overload of information. Similarly, Wang et al. (2014) described in their paper the use of physical markers in surgical applications as "invasive" and "error-prone".

3 MATERIALS & METHODS

This chapter provides a comprehensive overview of the materials and methodologies employed in the development of the AR guidance system application. Initially, a detailed presentation of the Microsoft HoloLens 2 is provided, followed by an in-depth examination of the Phantom 3D models, both of which constitute the core components of the experimental setup. Subsequently, the chapter delves into the specifics of Unity and Vuforia, clarifying their roles and functionalities within the framework of the thesis. In the second part of the chapter, the experimental setup designed to evaluate the system's accuracy is outlined. This is complemented by a description of the user study, which involved the participation of four surgeons, thereby providing insights into the application's efficacy in a real-world medical context.

3.1 Development of the AR guidance system for mandible osteotomies

3.1.1 Hardware

Microsoft HoloLens 2

To guide the surgeon in performing the osteotomies, the Microsoft HoloLens 2 OST HMD was used. Introduced in the previous section, it is an advanced MR headset that blends digital content with the physical world. It utilises immersive technology, including holographic lenses and spatial sensors, to enhance interactive experiences in various professional and creative applications. Holographic images can be overlaid onto the patient in the OR, aiding in surgical planning and allowing surgeons to navigate through the patient's unique anatomy with 'x-ray vision' (Dewitz et al., 2022).

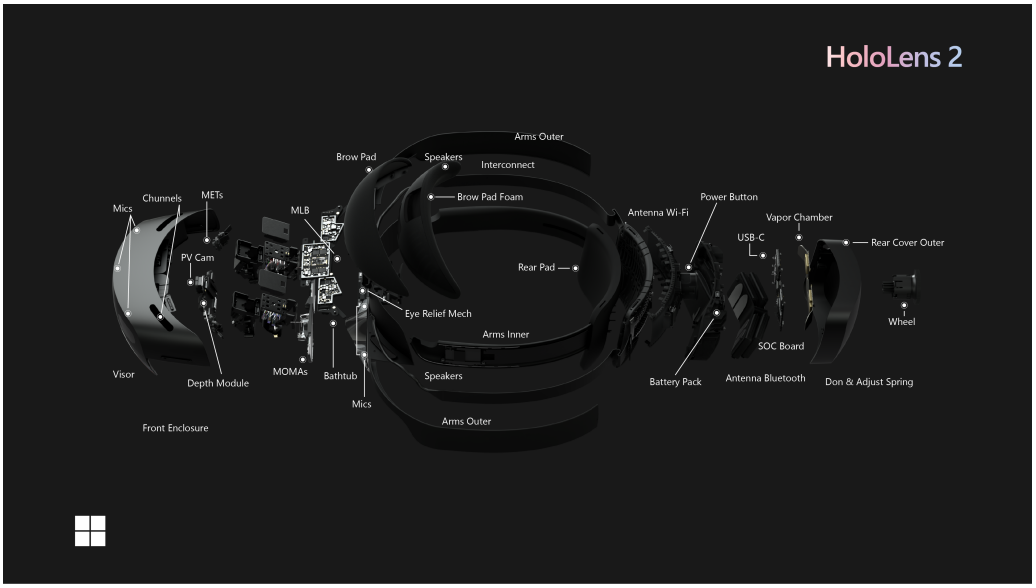


Figure 3.1: Exploded view of the Microsoft HoloLens 2 head-mounted device used in this developed AR application (Microsoft, 2023b).

The HoloLens 2 is equipped with see-through holographic lenses, known as waveguides, that offer a resolution of 2k 3:2 light engines per eye, ensuring a high-definition visual experience. The device's holographic density exceeds 2.5k radiants (light points per radian), providing a rich and immersive visual overlay. For depth perception and environmental interaction, the HoloLens 2 includes a time-of-flight (ToF) depth sensor, allowing accurate hand tracking and spatial mapping. The device's Inertial Measurement Unit (IMU), including an accelerometer, magnetometer and gyroscope, ensures precise head tracking. Additionally, an 8 MP RGB camera capable of capturing 1080p30 video is integrated into the device, along with four visible light and two IR cameras that facilitate accurate head and eye tracking. The audio experience in the HoloLens 2 is enhanced by a 5-channel microphone array and spatial sound speakers, enabling clear communication and immersive audio effects. The HoloLens 2 is also equipped with a Holographic Processing Unit (HPU) coupled with an ARM processor. The device also features a memory capacity of 4 GB DRAM and a storage space of 64 GB UFS 2.1. It supports Wi-Fi, Bluetooth 5.0, and USB-C (see figure 3.1). The HoloLens 2 is compatible with various applications built on the Universal Windows Platform (UWP), along with other MR applications. The device's battery life spans between 2-3 hours of active use, making it ideal for guiding surgeons in performing intraoperative osteotomies. For longer tasks, the device would need to be charged, using the USB-C fast charging capabilities. User interaction with the HoloLens 2 is led through direct hand-tracking manipulation of holograms, gaze tracking for control, and voice commands. This makes the user interface intuitive and user-friendly, making it ideal for this surgical application. In terms of design and comfort, the HoloLens 2 is constructed with carbon fibre and other lightweight materials, making it comfortable for extended use in the OR. It features an adjustable head strap and is designed to fit over glasses, ensuring accessibility for a wide range of users. The device's environmental understanding capabilities include 3D spatial mapping and spatial anchors, which allow holograms to keep their position in the real world. Finally, the HoloLens 2 ensures user security through Windows Hello iris recognition, offering a secure and personalised access system. These specifications collectively illustrate the HoloLens 2's capacity to create a dynamic and interactive surgical MR experience (Microsoft, 2023b).

Phantom 3D models and Cutting Guides

For testing the developed system, phantom mandible 3D-printed models are used. These aim to replicate the anatomical intricacies of human mandibles with precision. The production process starts with acquiring medical imaging data, derived from CT scans of the patient's mandible. Through the use of specialised image segmentation software, .stl files of the 3D mandible model were provided anonymously by the University Hospital of Antwerp (see figure 3.2).

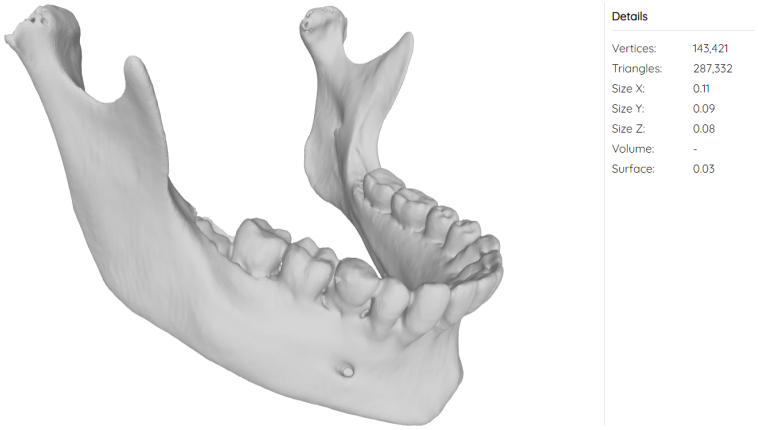


Figure 3.2: 3D model of the mandible provided by the UZA, derived from CT Scans of an anonymised patient.

Four custom-made cutting guides are designed to later compare the proposed system with the state-of-the-art method (see figure 3.3). Subsequently, the models are 3D-printed in the Robot Assisted Surgery (RAS) lab in KU Leuven. The material used is white polylactide (PLA), chosen for its accessibility, ease of use and adapted strength. The use of phantom mandible models in this work adheres to medical ethical guidelines, all data received were anonymised and acquired with appropriate consent.

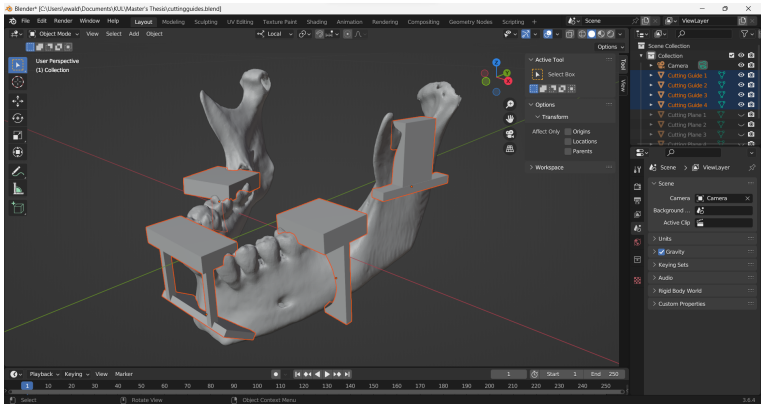


Figure 3.3: Design of the cutting guides in Blender through the 'boolean' tool, to perfectly fit the patient-specific mandible shape.

3.1.2 Software

Unity

To develop the application on the HoloLens 2, Unity Engine is used. Unity is a game engine and development platform, used for its capabilities in creating both 2D and 3D interactive content. The programming language of Unity is primarily C#, known for its power and flexibility, facilitating a wide range of development needs. The asset pipeline in Unity is particularly noteworthy, allowing for the easy import and integration of various tools such as the Mixed-Reality Toolkit (MRTK) or Vuforia described below. Another significant advantage of Unity is that it supports many different operating systems such as Windows, macOS, Linux, iOS, Android, and various AR/VR platforms, making it compatible with many HMDs. When it comes to developing applications for the HoloLens, the integration of the MRTK with Unity significantly enhances its capabilities. It offers HoloLens-specific features like spatial mapping, hand tracking, and gaze tracking, which are essential for creating realistic MR experiences. The toolkit includes a flexible input system that can be adapted for various interaction modalities, including gestures and voice commands, enriching the surgeon's interaction with the application. Moreover, the MRTK provides a suite of pre-built UI components and interaction patterns specifically designed for MR environments. This is complemented by enhanced spatial awareness, allowing for a more realistic and interactive blend of digital and physical environments. Performance optimisation is another critical aspect of the MRTK, ensuring that applications run smoothly on the HoloLens (Microsoft, 2023a). Finally, the extensive documentation and the supportive community of developers around Unity is a valuable resource, offering guidance, troubleshooting, and best practices for good application development (Unity, 2023).

For this framework, the Unity 2022.3.9f1 version is used for creating the AR application. The app is built and released to the HoloLens 2 through version 17.8 of Microsoft Visual Studio Integrated Development Environment (IDE).

Vuforia Engine

Vuforia is a software development platform implemented through Unity that promotes the creation of interactive and immersive augmented reality experiences (Estrada et al., 2022). Owned by PTC ©, the Vuforia tool allows for powerful image or object recognition and tracking possibilities. Extensively used in industry, healthcare or manufacturing, the SDK provides a large choice of applications, making it a popular choice for AR-oriented solutions (PTC, 2023).

Vuforia works by first recognising a predefined target. The tool then overlays virtual content onto the physical world environment. The targets can be decomposed into three categories depending on the application: Images, Environments, and Objects (see figure 3.4).

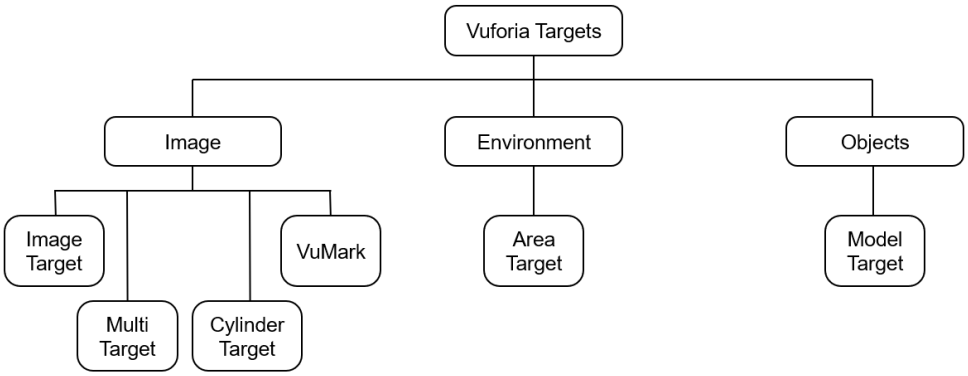


Figure 3.4: Overview of the main Vuforia Targets by categories. Image, Environment and Objects targets with their subclasses.

Images: This target category groups different marker-based targets. The Image Target (simple flat images, such as ArUco or ChArUco markers), Cylinder Target (wrapped image into a cylindrical shape), Multi Target (Image Target arranged in regular geometry shapes, such as a cube), VuMark (customized markers designed for unique identification). A Cloud Recognition Service is suggested for getting optimal recognition performances.

Environments: The Area Target feature lets you scan a room or other environments to accurately align virtual content in various pre-defined places.

Objects: This last category is the most interesting one for this work and will be the one used in this thesis. It contains the Model Target feature, a powerful tool used to recognise and track objects by shape, using existing 3D models. Section 3.1.3 describes how the tool is used to track the mandible.

The Vuforia 10 API typically consists of 3 key components. Engine, Observer/Observation and Controller (figure 3.5).

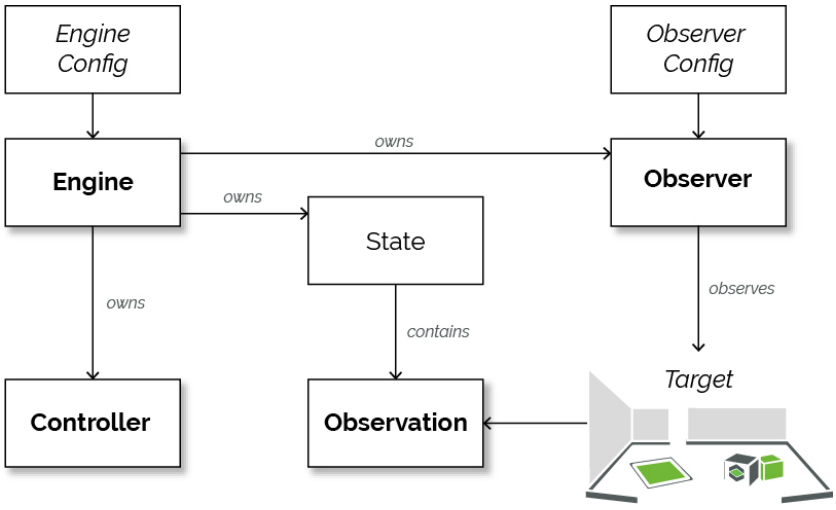


Figure 3.5: Vuforia 10 Application Programming Interface (API) (Vuforia, 2023).

The Engine manages Vuforia's lifecycle. It allows to create, start, stop or destroy the augmented reality application. Camera or rendering parameters are configured through the VuforiaBehaviour instance in Unity, although a default configuration is provided with the tool. The Observer provides components that are created to observe properties from the real world (Targets). For this thesis, the Model Target Observer is used to recognise 3D mandibles based on a Computer-Aided Design (CAD) model (see section 3.1.3). In practice, these are managed in Unity through target behaviour components that are attached to GameObjects. As users interact or change the AR scene, the changes reported by the Observers between two frames are known as 'Observations' and are stored in the State. This includes pose, status or mesh data from the Observations made by the Observer as well as camera and rendering data. Finally, the Controller is used to tune the Engine and other settings in real-time. The default configurations will be used here (Vuforia, 2023).

3.1.3 Markerless tracking of the mandible

The registration between the physical and virtual models is achieved through a tracking algorithm, implemented by employing the Model Target functionality of Vuforia, a markerless tool used to recognise and track physical objects in the real world. Here is an overview of how it is implemented (figure 3.6).

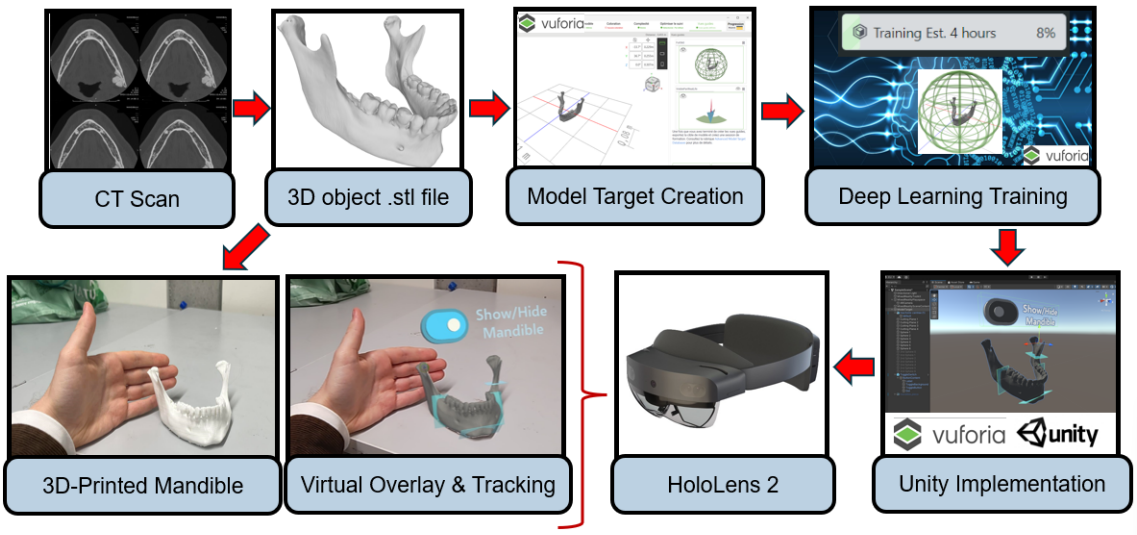


Figure 3.6: Process layout of the proposed markerless guidance system. From the patient's CT Scans to real-time virtual overlay and tracking.

A 3D model of the physical object we want to identify and accurately track is acquired. Here, the 3D model of the mandible segmented and 3D-reconstructed earlier from CT Scans is used. In this framework, the 3D model is imported into Vuforia's Model Target Generator (MTG), where an Advanced Model Target is created, allowing for recognition of the model from multiple positions and angles, rather than just one. This approach is essential for mandible reconstruction surgery, where varying views of the mandible are necessary. Specifically, a combination of 'Full 360°' and 'Constrained Angle Range' Advanced Views is used to simulate real surgery conditions, enabling the system to recognise the mandible within specified elevation and azimuth angle ranges (see

figure 3.7).

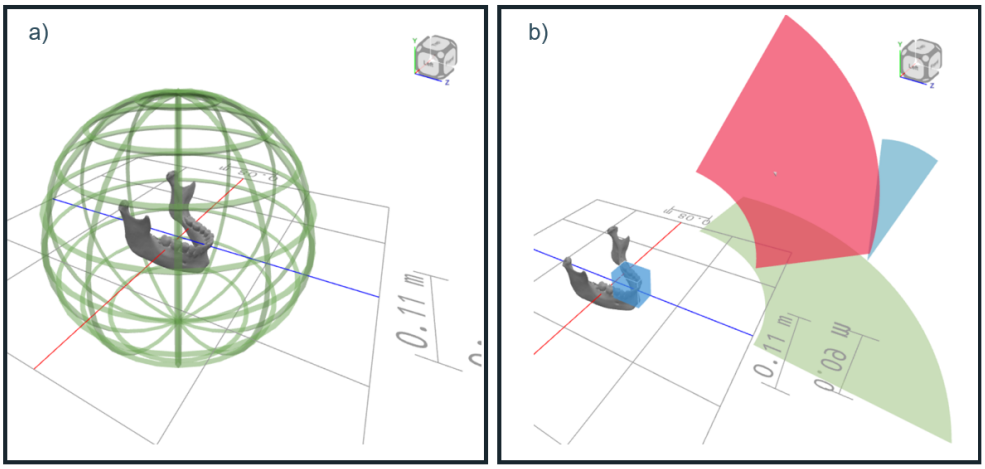


Figure 3.7: Configuration of the Advanced View in the Vuforia's Model Target Generator (MTG) app. a) 'Full 360' Advanced View; b) 'Constrained Angle Range' Advanced View.

Upon creating the Advanced Model Target and Views of the mandible in the MTG, a database with model details is generated and uploaded to Vuforia's cloud for deep learning training (see figure 3.8). Here, machine learning algorithms analyse the mandible's unique features, enabling the system to recognise it from various angles (VuforiaMTG, 2023).

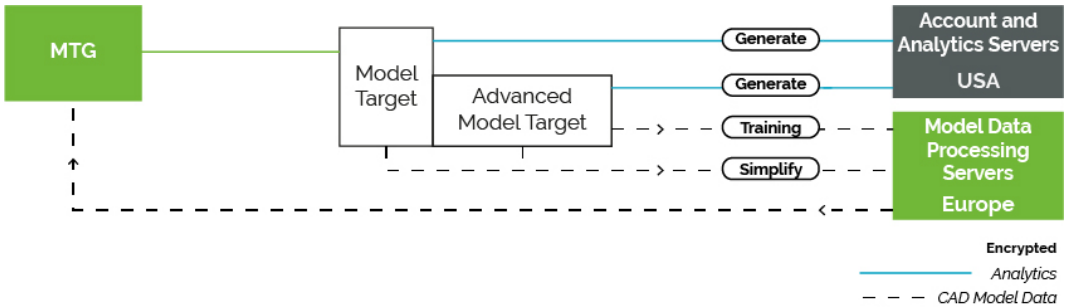


Figure 3.8: General overview of the data flow between the Vuforia servers in Europe and the MTG app when training the Advanced Model Target Database.

The training time for the mandible model target, which features Advanced Views and consists of 287,332 mesh triangles, takes around 4 hours. The outcome is a comprehensive database ready for use in Unity, enabling robust recognition and tracking of the mandible. While the deep learning training time varies for different patients or models used, the overall process can be executed in only a few hours. This provides a strong advantage compared to the current cutting guide method, which takes several weeks to complete the whole design and 3D printing process (Goormans et al., 2019).

User experience (UX) and UI are kept as simple and intuitive as possible, to avoid any distraction and allow the surgeon to fully focus on its task. In Unity, the Model Target integrated into the scene as a GameObject is linked to the mandible's trained database. Virtual content is associated with this GameObject. Here, a virtual replica of the mandible is precisely aligned with the model. Addi-

tionally, four cutting planes are introduced (see figure 3.9), which, although chosen arbitrarily here, can be derived from preoperative planning to indicate precise cutting trajectories to the surgeon. The user can hide or show the virtual mandible through a simple UI containing a toggle switch.

The HoloLens' cameras scan the environments. If it detects the physical object based on the 3D model and its database, it will overlay the chosen virtual content on top of the real-world object and track its movements. The system updates the position changes at every frame, meaning that the mandible model can be handled and moved around freely while keeping the hologram at its expected position.



Figure 3.9: User's point of view of the proposed guidance system. The HoloLens detects the mandible Model Target (left); The HoloLens displays the virtual content on the scene, including the virtual mandible, four virtual cutting planes, and a virtual toggle switch (right).

The framework presented in figure 3.6 illustrates a modular process layout for markerless tracking of the mandible, where each block represents an independent stage. Due to its modular nature, individual components such as the 3D model chosen (the mandible), the tracking technology (Vuforia), the software development platform (Unity) or the HMD (HoloLens 2) can be changed or updated without affecting the overall structure. This adaptability makes the framework versatile, allowing it to be customised for different patients or even different surgical procedures, but also compatible with various HMDs, globally suitable for integration with other software and hardware systems.

3.2 Experimental setup for accuracy measurement and user study

3.2.1 Hologram Registration accuracy

A method to quantitatively assess the registration accuracy of the hologram on the real mandible is described. Based on a method proposed by Palumbo et al. (2022), it measures the alignment error of a fixed point on the mandible to six virtual concentric spheres of known size and position. The

exact position of the point was obtained by selecting the highest node of the mandible's coronoid process[1] in Blender and matching the corresponding coordinates in Unity for the spheres' centre.

The position of the physical point, relative to where it falls within the projected holographic spheres, indicates the error. This is determined with the virtual spheres that have radii ranging from 1 mm to 6 mm. As seen in Figure 3.10, when the physical point is perfectly aligned with the centre of the virtual spheres, the error is considered to be 1 mm. If the point lies in the sphere with a radius of 3 mm, the error is 3 mm.

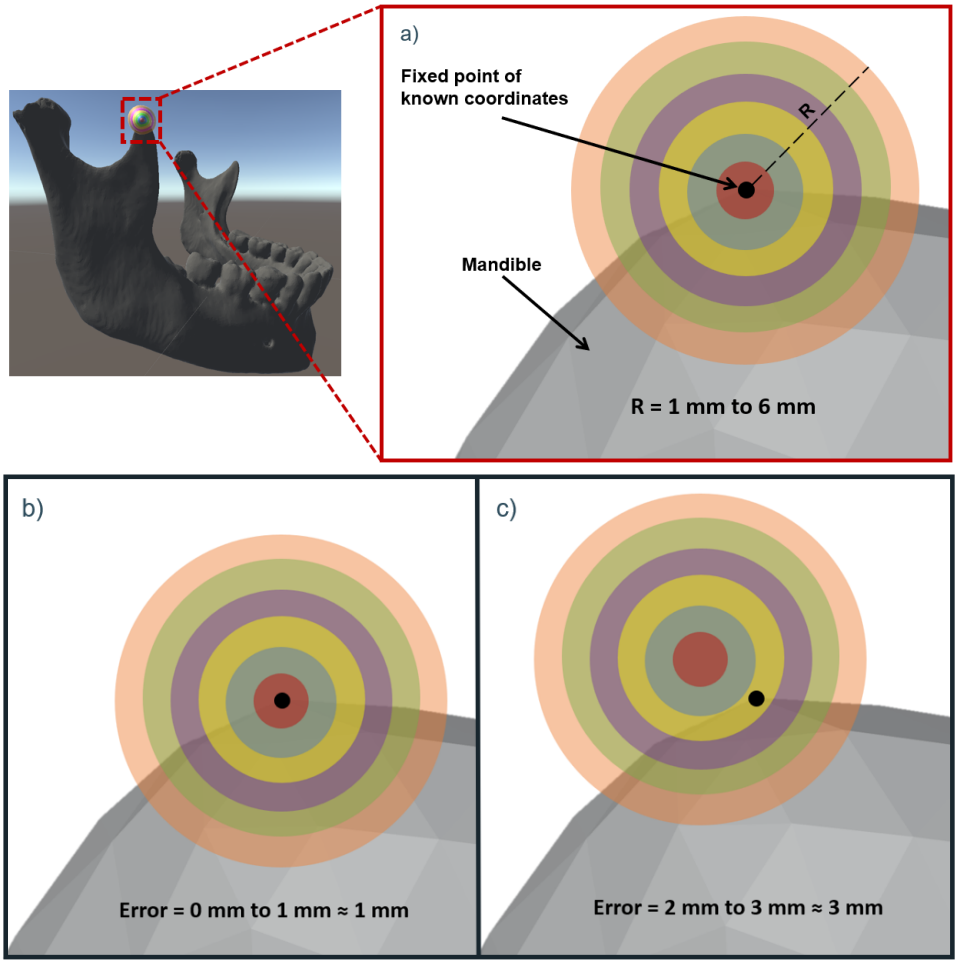


Figure 3.10: Hologram accuracy assessment method. a) coloured virtual concentric spheres projected on the mandible and perfectly aligned with the fixed physical dot. Virtual components are shown in colour, while real physical components are shown in grey or black; b) example of a situation giving an approximate error of 1 mm; c) example of a situation giving an approximate error of 3 mm.

For this registration accuracy evaluation procedure, an inter- and intra-operator assessment was performed: one user performed the Hologram registration accuracy procedure 5 times under different lighting conditions (standard, dull surgical and bright surgical, as pictured in figure 3.11) and

[1]The mandible coronoid process is the bony surface located on the superior part of the ramus. It serves as an attachment point for muscles involved in jaw movement (Breeland et al., 2023)

different coverage of the mandible (25% and 50% of the mandible covered by a piece of paper), and 4 surgeons performed the Hologram registration accuracy procedure once under standard lighting conditions. While the ”standard lighting conditions” were slightly different for the intra- and inter-operator assessments (i.e. performed in different rooms), they will be considered equivalent.

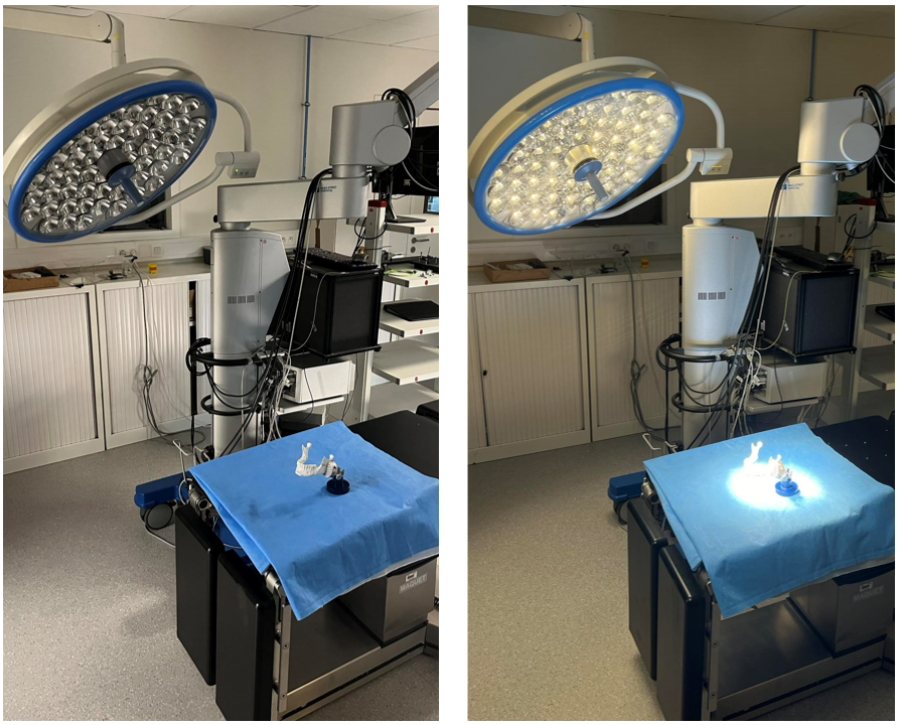


Figure 3.11: Hologram accuracy intra-operator assessment setup. Mandible illuminated under standard lighting condition (left); bright surgical lighting condition (right).

The mandible was attached to a fixed clamp for precision and consistency throughout the tests. Furthermore, to account for the three-dimensional geometry of the mandible, each test involved measurements from 3 different viewing angles: one from the side of the mandible, one from the top and one from the front of the mandible. The ”HoloLens 2 eye calibration” was run for every user to ensure correct alignment before each test.

3.2.2 User study

The upcoming user study was a crucial part of this thesis. As the primary end-users, surgeons can bring valuable insights and feedback on the system. It was then important to engage directly with them to test the application and assess whether the requirements were met and whether the limitations were properly defined.

To that matter, the four surgeons participating in the study were asked to accurately draw osteotomy lines on a model mandible. On one side, the proposed markerless AR guidance system was used to guide the surgeons in performing the task in real-time with the HoloLens 2 (figure 3.12, left). Then, the state-of-the-art method involving the physical cutting guides was also performed

for comparison. For this, the custom-made cutting guides described above were placed on the mandible by the surgeons, and a thin red line was drawn on the mandible following the guide (figure 3.12, right).



Figure 3.12: A surgeon drawing the osteotomy planes on the model mandible with the HoloLens 2, in the context of the user study (left); State-of-the-art method for drawing the osteotomy line with the custom-made cutting guides. These latter are notched to perfectly fit the shape of the mandible (right).

The key objectives of this user study were twofold. First, the precision and accuracy of both guiding approaches were compared together, assessing how easily the surgeons could follow the planned osteotomy planes. For that matter, each drawn osteotomy line was subsequently recorded with the tip of an electromagnetic (EM) sensor, generating a point cloud of the obtained measurements (see figure 3.13), using Python (Appendix A). For each mandible, 20 points were recorded along each pair of osteotomy lines. The Euclidean distance between each pair of points is then calculated as shown in figure 3.14, using this formula:

$$d_i = \sqrt{(P_{Gx_i} - P_{Hx_i})^2 + (P_{Gy_i} - P_{Hy_i})^2 + (P_{Gz_i} - P_{Hz_i})^2} \quad \forall i \in [1,20] \tag{3.1}$$

Where P_{Gx_i} represents the x-coordinate of the i^{th} point on the line drawn with the cutting guide, and P_{Hx_i} represents the x-coordinate of the i^{th} point on the line drawn with the HoloLens. The mean error per pair of lines is then averaged across the 20 values as such:

$$\delta = \frac{\sum_{i=1}^{20} d_i}{20} \tag{3.2}$$

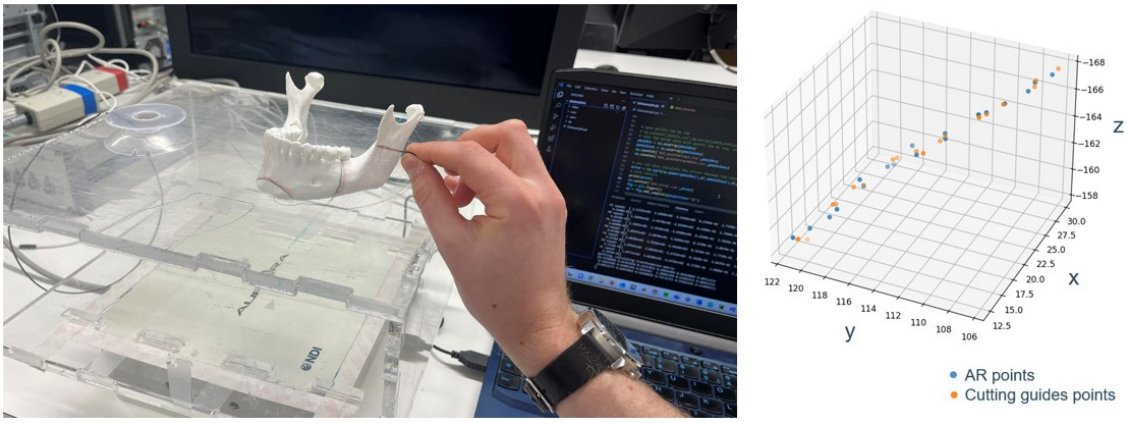


Figure 3.13: Points acquisition with the EM sensor of the second mandible, first osteotomy line of the first surgeon during the user study (left); and its associated point cloud recorded through Python (right).

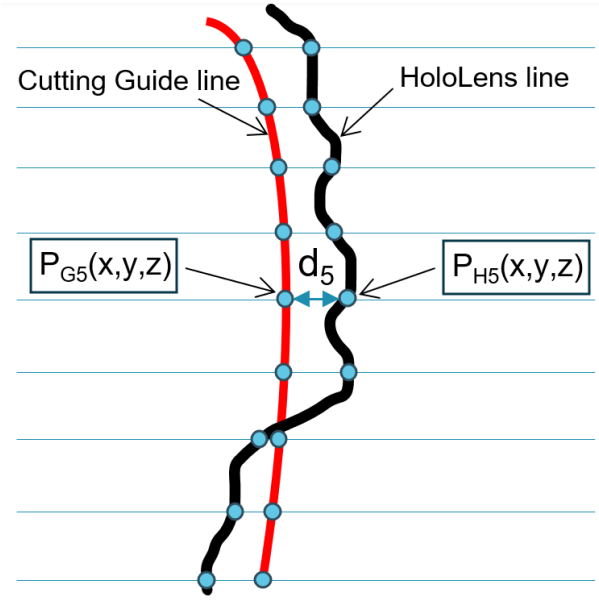


Figure 3.14: Scheme of the distance calculation between two points of the points cloud. The distance d_5 between the 5th pair of points is shown as an example.

As a second objective, the usability and efficiency of the developed system were evaluated, assessing how the method with the HoloLens compares to the state-of-the-art one, considering the overall user experience, learning curve, and challenges faced. This was evaluated through a post-test questionnaire, containing feedback questions and the NASA Task Load Index (TLX) assessing the workload felt by the surgeons when completing the task with the HoloLens 2 (Appendix B). The six workload factors are evaluated equally (i.e. with the same weight factor (Byers et al., 1989)) as follows: mental and physical demand assess respectively how mentally and physically demanding was the task. The temporal demand factor gives an idea of how hurried or rushed was the pace of the task. The performance factor evaluated how successful the user felt when accomplishing what was asked to do. The effort criterion measures how hard the user had to work to accomplish

the expected level of performance. Finally, the frustration factor assesses how irritated, annoyed, stressed, discouraged or insecure the user felt while performing the task (NASA, 2020). The individual scores are then recorded on a scale from 0 to 100, and an overall score per factor is calculated with equal weight.

4 RESULTS

4.1 Accuracy of the registration

This section provides the results obtained through the inter and intra-operator accuracy assessment, using the ”sphere method” described above. The experiments aimed to measure the alignment error by observing the deviation of a fixed point on the mandible from its expected position within a set of virtual concentric spheres. This method effectively quantifies the registration accuracy by noting the radial distance of the point from the centre of the spheres, with a perfect alignment corresponding to an error of 1 mm or less.

4.1.1 Inter-operator accuracy

For the inter-operator assessment experiment, the four surgeons had to look at the spheres and tell the assessor where the fixed black dot on the physical mandible was perceived through the HoloLens 2. The results in table 4.1 are colour-coded, representing the perceived alignment of the dot in one of the six virtual spheres, with ”RED” indicating an alignment error of 1 mm or less, and ”BLUE” indicating a larger error, between 1 and 2 mm (see figure 3.10).

Surgeons 1, 2, and 3 demonstrated a high degree of precision in the front and side views with an error of 1 mm. The same surgeons, however, exhibited varying degrees of accuracy in the top view. Surgeon 2 observed a larger error margin, suggesting a 2 mm deviation, while Surgeons 1 and 3 maintained their observed 1 mm accuracy. Surgeon 4, in contrast, consistently showed a larger deviation of 2 mm across all views. The maximum mean accuracy for the inter-operator assessment for the four surgeons across the different views is 1.33 mm.

	Surgeon 1	**Surgeon 2**	**Surgeon 3**	**Surgeon 4**
Front View	RED (1 mm)	RED (1 mm)	RED (1 mm)	BLUE (2 mm)
Side View	RED (1 mm)	RED (1 mm)	RED (1 mm)	BLUE (2 mm)
Top View	RED (1 mm)	BLUE (2 mm)	RED (1 mm)	BLUE (2 mm)

Table 4.1: Results of the inter-operator accuracy assessment, with ”RED” indicating an alignment error of 1 mm or less, and ”BLUE” indicating an error between 1 and 2 mm.

4.1.2 Intra-operator accuracy

The intra-operator accuracy assessment was conducted under three different visibility conditions: the standard condition with no obstruction, and two additional conditions where 25% and 50% of

the mandible were covered, obstructing the view to varying degrees. The evaluation was repeated five times by a user to ensure the reliability of the results. The ”dull” and ”bright” surgical lighting conditions were found to be impractical (see figure 4.1), thus will not be accepted as valuable results. Hypothetical reasons for such conclusions will be further discussed later.

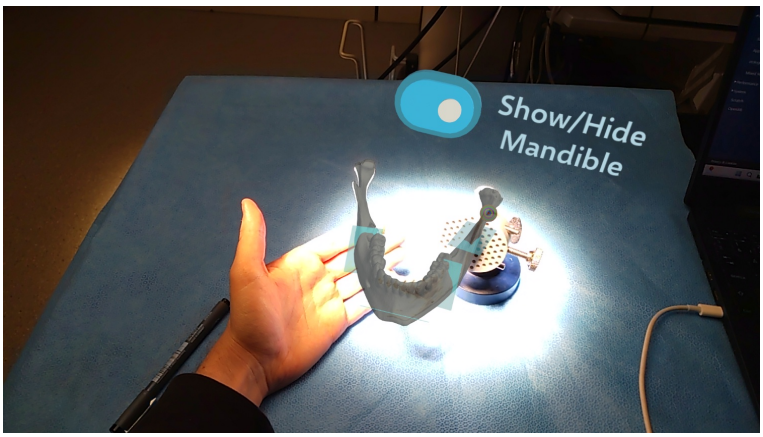


Figure 4.1: User's Point Of View (POV) of the Hologram accuracy intra-operator assessment under impractically bright surgical lighting conditions.

From table 4.2, in the standard, unobstructed condition, the average alignment error was 1.20 mm, 1.20 mm, and 1.40 mm for the front, side, and top views, respectively. This suggests a slight variation in registration accuracy depending on the perspective, with the top view exhibiting a marginally higher error rate. The maximum mean accuracy for the intra-operator assessment across the different views, and under the different covering conditions is 1.40 mm.

When a quarter of the mandible was covered, the average error increased, indicating a direct impact of visibility on registration accuracy. The front view showed a significant increase in error to 2.20 mm, while the side view had a minimal decrease to 1.00 mm, and the top view presented an error of 1.20 mm. With half of the mandible covered, the error rates varied further. The front view's accuracy decreased, with an error of 2.00 mm. The side view error increased to 1.40 mm, reflecting an expected trend of diminished accuracy with greater obstruction. Conversely, the top view registered a decreased error of 1.00 mm, suggesting an atypical pattern where visibility constraints may not linearly correlate with registration accuracy.

	Standard [mm]	**25% Covering [mm]**	**50% Covering [mm]**
Front View	1.20	2.20	2.00
Side View	1.20	1.00	1.40
Top View	1.40	1.20	1.00
Total	1.27	1.47	1.47

Table 4.2: Results of the intra-operator accuracy assessment.

It is also important to add that the initial registration time (i.e. the time taken for the Hologram to initially appear) was greater when the mandible was covered than in standard conditions (table 4.3). However, the registration time when viewing the mandible from the side does not vary much across the different situations (around 1 second).

	Standard	25% covering	50% covering
Front view	1.0 sec.	1.8 sec.	2.2 sec.
Side view	1.0 sec.	1.1 sec.	1.1 sec.
Top view	1.2 sec.	2.2 sec.	3.8 sec.

Table 4.3: Average initial registration time for standard lighting conditions and partial covering of the mandible, during the intra-operator accuracy assessment.

4.2 Cutting accuracy

This section provides the results obtained through the user study involving the 4 surgeons, as described above. First, the precision and accuracy results are shown. These are obtained through the error measurement as explained in section 3.2.2. Then, the usability and efficiency of the system is depicted through the NASA TLX survey results, in parallel with the custom questionnaire provided to the surgeons after the user study.

4.2.1 Precision and accuracy

During the user study, 4 surgeons were each asked to draw 4 pairs of osteotomy lines on 3 mandibles. After the experiment, the 12 mandibles (see figure 4.2) were taken back to the lab, and the average distances between each pair of lines (i.e. one line with the HoloLens and one line with the custom-made cutting guides) were recorded using an EM sensor.



Figure 4.2: Final result of the user study. The 12 mandibles, the 4 custom-made cutting guides and the 48 pairs of drawn osteotomy lines.

The results in table 4.4 indicate a minimum error that was consistent across all surgeons, with a low of approximately 0.03 mm. However, the maximum error highlighted a disparity in precision, particularly with surgeons 2 and 4, who recorded the highest deviation at respectively 4.02 mm and 4.03 mm. Surgeon 2's results were notably less consistent than the others, with an average

deviation of 1.64 mm, double that of the most precise surgeon in this task, who averaged 0.82 mm. The standard deviation (σ) further accentuates this point; surgeons 1 and 3 demonstrated a high level of precision with standard deviations of 0.55 mm and 0.53 mm, respectively, indicative of results that closely clustered around their average values. Conversely, surgeon 2's results were more scattered, as evidenced by the highest standard deviation of 1.21 mm.

When examining the overall data, the total average error was calculated at 1.08 mm with an overall standard deviation of 0.94 mm.

	Min. [mm]	**Max. [mm]**	**Mean [mm]**	**σ [mm]**
Surgeon 1	0.03	1.82	0.83	0.55
Surgeon 2	0.64	4.02	1.64	1.21
Surgeon 3	0.03	1.43	0.82	0.53
Surgeon 4	0.12	4.03	1.03	1.10
Total	0.03	4.03	1.08	0.94

Table 4.4: Results of the user study accuracy across the four surgeons. The minimum, maximum, mean values and the standard deviation (σ) are shown in mm.

Table 4.5 provided shows the precision of the osteotomy lines drawn across the four different planes. For Plane 1, the minimum distance recorded was 0.16 mm, and the maximum was 4.02 mm, with an average of 1.57 mm. The standard deviation was 1.28 mm, suggesting a relatively wide spread of values around the mean as seen in figure 4.3. Plane 2 showed similar results with a slightly higher maximum error of 4.03 mm and a comparable average of 1.59 mm. The standard deviation was lower than Plane 1 at 0.89 mm, which indicates a tighter grouping of measured distances around the mean, suggesting slightly greater consistency in this plane compared to Plane 1. Plane 3 shows improved precision with the smallest maximum error of 1.27 mm and the lowest of 0.71 mm. The standard deviation of 0.34 mm was also the lowest among the four planes, reflecting a high level of consistency in the surgical task on this plane. Plane 4 also showed great precision with a maximum error of only 0.93 mm and the lowest average of 0.46 mm. The standard deviation was comparable to Plane 3 at 0.31 mm.

	Min. [mm]	**Max. [mm]**	**Mean [mm]**	**σ [mm]**
Plane 1	0.16	4.02	1.57	1.28
Plane 2	0.34	4.03	1.59	0.89
Plane 3	0.03	1.27	0.71	0.34
Plane 4	0.03	0.93	0.46	0.31
Total	0.03	4.03	1.08	0.94

Table 4.5: Results of the user study accuracy across the four planes. The minimum, maximum, mean values and the standard deviation (σ) are shown in mm.

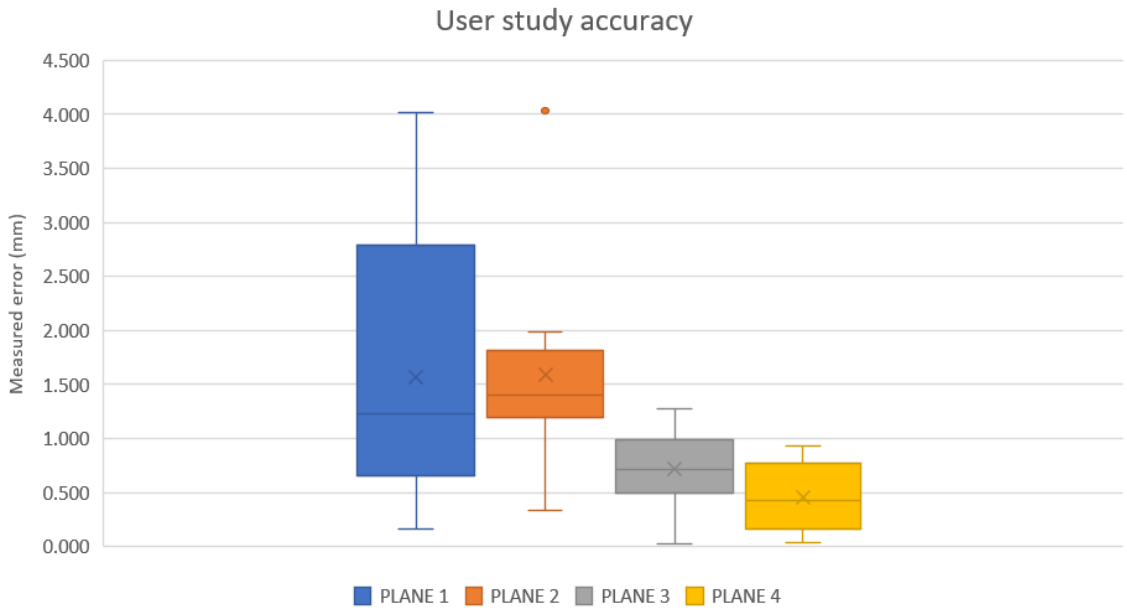


Figure 4.3: Box plot showing the measured error across the four different planes.

4.2.2 Usability and efficiency

This section gives the results of the questionnaire given to the surgeons after their experiment. It included the NASA TLX as well as open questions related to potential feedback on the system. The detailed results can be found in Appendix B. The recorded duration of every experiment is also provided below.

NASA Task Load Index (TLX)

Figure 4.4 summarises the workload experienced by the surgeons when performing the user study. The mental, physical and temporal demands were evaluated, as well as the performance, effort and frustration felt by the surgeons when executing the task. The six factors are then averaged across the four surgeons and the result is shown in figure 4.5.

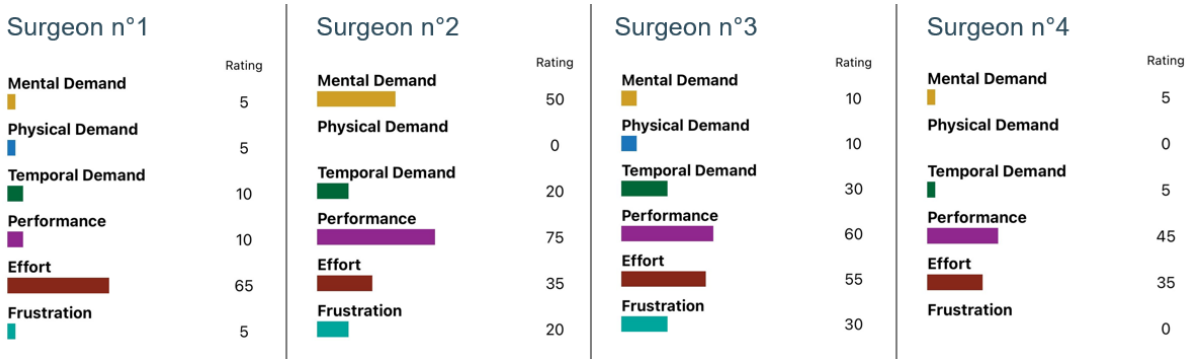


Figure 4.4: Individual NASA Task Load Index results for each factors.

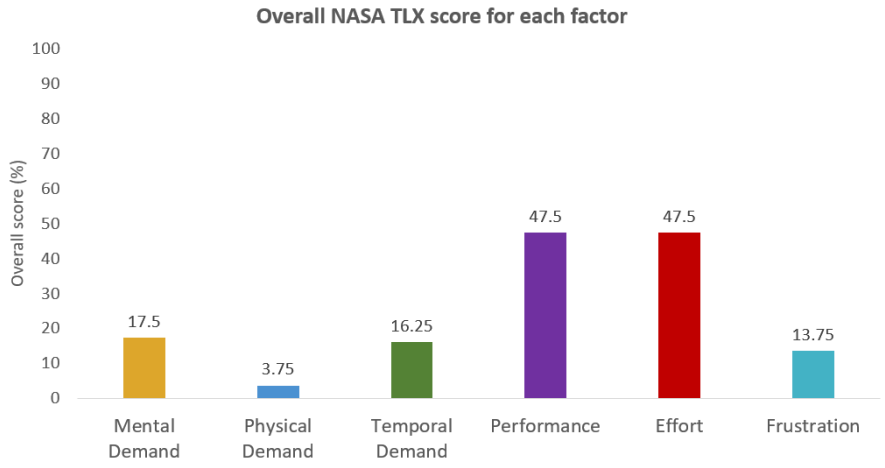


Figure 4.5: Overall NASA Task Load Index results for each factors.

Overall, the surgeons experienced very low physical demand on the task (scoring 3.75 out of 100), low frustration (13.75%) as well as low temporal (16.75%) and mental demand (17.5%). However, in comparison, the surgeons did not feel very confident with their performance (scoring 47.5 out of 100) and experienced some effort to reach their expected level of performance while executing the task (47.5% as well).

Questionnaire on the usability of the system

For the question ”Is there anything you liked during this experiment”, the 1st surgeon liked the novelty and the perceived accuracy of the system. The 2nd surgeon thought the system was very educational and could even be used for practising before an operation. The 3rd surgeon thought the system had ”great potential”, while the last surgeon found it ”astonishingly accurate”. The latter also expressed that he had never used AR before.

Suggestions of improvement include higher resolution of the cutting planes, introducing ”opacity sliders” to adjust the visibility of certain holograms, or changing the cutting planes with cutting lines to enhance visibility. The 1st surgeon also suggested a better 3D printing quality (resin prints) for further drawing precision.

Temporal considerations

The average time taken to draw the osteotomy lines was 237.75 seconds for the first mandible. The second one took an average of 142.5 seconds, while for the 3rd mandible, the surgeons took an average of 106 seconds to complete the four osteotomy lines. The cutting guide method took on average 94 seconds to be completed (see table 4.6 for details).

	Surgeon 1	**Surgeon 2**	**Surgeon 3**	**Surgeon 4**
Mandible 1	4 min 13 s	3 min 51 s	2 min 57 s	4 min 50 s
Mandible 2	2 min 15 s	3 min 15 s	2 min 45 s	1 min 15 s
Mandible 3	2 min 11 s	1 min 03 s	2 min 15 s	1 min 35 s
Cutting Guides	1 min 31 s	2 min 13 s	1 min 05 s	1 min 27 s

Table 4.6: Time taken by the four surgeons to draw the four osteotomy lines. Results with the HoloLens (for three mandibles) and without the HoloLens (with custom-made cutting guides).

5 DISCUSSION

In this pivotal section of the thesis, the implications of the findings are discussed, reflecting on the future integration of augmented reality in maxillofacial surgery. The goal of this thesis was to establish a markerless AR guidance system for mandible reconstruction surgery using the Microsoft HoloLens 2. Principal requirements included real-time tracking and registration, few additional hardware components and a registration accuracy under 2 mm. Not only these requirements were met, but the resulting framework opened a path to new perspectives that can be further extended to other surgical domains.

Building upon the methods outlined in a former student master's thesis from KU Leuven (Wybaillie (2022)), which focused on integrating AR in mandibular reconstruction surgery, the proposed framework enhanced the methodologies significantly. Going beyond the expected scope, an innovative method to improve the previous framework is proposed. Furthermore, comprehensive assessment protocols and in-vitro tests were developed, consequently exceeding the initial expectations set for the project.

By looking over the calculated hologram shift of less than 1.37 mm and the accuracy of 1.08 mm obtained following the user study, the precision of the system is thoroughly discussed. Moreover, the insights gathered from the surgeons' in-vitro experiences provide a perspective on the adaptability and practicality of the proposed framework in a surgical environment.

5.1 Precision of the system

The state-of-the-art cutting guide method for maxillofacial surgery through the fibula free flap harvesting gives a mean error of 2.60 mm between the Virtual Surgical Planning and the resulting osteotomies (Pietruski et al., 2019). Goormans et al. (2019) compared mandibular osteotomies to their respective virtual plans and obtained a length deviation of 1.74 mm. This is still well above the obtained accuracy results of 1.08 mm in this work. It is worth mentioning that the latter represents the mean error between the osteotomy lines drawn with the custom-made cutting guides and the ones drawn with the AR application, and not a direct comparison with the AR and the VSP.

The results obtained through the inter- and intra-operator assessments showed how accurately the proposed AR application registers virtual objects in the real world. The results demonstrated a maximum mean accuracy of 1.37 mm, indicating the potential effectiveness of the AR system for surgical applications. Moreover, while the "standard lighting" conditions were different (i.e. not performed in the same room) for the intra- and inter-operator assessment, similar results were obtained.

The collected data from the inter-operator assessment indicate that while the spatial guidance

system has the potential to provide a high level of accuracy (as seen with the RED-coded results in table 4.1), there are slight discrepancies in the precision levels between different surgeons and different views. The consistent BLUE-coded results for Surgeon 4 could reflect individual variability in using the system or could highlight potential limitations in the guidance system's ability to provide uniformly accurate information to different operators.

The intra-operator assessment experiment revealed some particularities that are worth further attention. First, all the measurements were performed under "standard light conditions" (cfr figure 3.11, left). Indeed, as can be seen in figure 4.1 and on the right side of figure 3.11, the reflection caused by the surgical light made the measurements impractical. A possible reason for this could be due to the saturation of the HoloLens' camera, being over-exposed to light due to the reflection, thus complicating the recognition of the Model Target. A second particularity can be seen when partially covering the mandible. Indeed, while the side and top views gave good accuracy results (around 1.15 mm), the front views showed less convincing results when partially covered (around 2.10 mm). Finally, a higher registration time was recorded for the top and front views when partially covering the mandible. This could be due to the recognition algorithm receiving fewer points compared with the database information, thus taking more time to initiate the registration. However, while taking more initial registration time on average, the top views of the partially covered mandibles gave a convincing accuracy (around 1.10 mm). From these observations, it can be concluded that the best accuracy and registration performances were obtained under standard lighting conditions, and by viewing the mandible from the side.

The user study yielded a convincing accuracy of 1.08 mm. When compared to the other approaches described previously, the proposed system seems to be promising. Indeed, to the author's best knowledge, this is the first system that offers real-time markerless tracking of the patient's mandible, achieving a registration accuracy of less than 1.50 mm. Furthermore, it facilitates multi-angular tracking of the patient's mandible, thereby providing the surgeons with the flexibility to adjust their position comfortably throughout the surgical procedure.

Looking at the user study's results, some osteotomy planes seemed to be harder to follow for the surgeons. When looking at the tables, planes 1 and 2 appear to result in a higher error (respectively 1.57 mm and 1.59 mm) than the others (0.71 mm and 0.46 mm). To investigate this even further, we can look at the standard deviation of these values across the different planes. Figure 4.3 suggests that plane 1 has a high standard deviation (i.e. largely spread values around the mean). This can be explained by the outliers obtained by the 2nd Surgeon, possibly due to an error in calibration with the HoloLens 2. Plane 2, however, shows consistent and relatively high error values. In conclusion, plane 2 seems to be the hardest to follow accurately. This could be due to its non-optimal placement on the mandible, with a possible error-prone drawing path.

More generally, it seems that the accuracy can be further improved. Indeed, apart from the outliers values obtained by the 2nd surgeon, these error measurements are the result of surgeons with little AR experience. Furthermore, feedback from the users suggested a higher hologram resolution and better 3D-print quality, which could potentially improve the results.

5.2 Scalability and future prospects

As we move forward, the field of augmented reality in maxillofacial surgery stands on the corner of innovative change. The current possibilities offered by AR could revolutionise how surgical procedures are planned and executed. While none of the AR-based registration methods proposed thus far have been implemented in real surgical environments, future developments are expected to focus on bringing AR closer to the OR. With this goal in mind combined with the possibilities offered by the proposed framework, future work will focus on a few key aspects. As an important remark, figure 3.6 showed an overview of the implemented process. These building blocks have the advantage of being independent and replaceable, which will be a central point of the following discussion.

First, a focus on solving the lighting problem described in this work will be evaluated in future works. While the standard conditions tested in this framework gave convincing results, other surgery-specific conditions must be tested. This would include changing surgical light conditions to test the application's robustness, while possibly implementing camera filters on the HMD for less light reflections. Furthermore, as suggested by the surgeons during the user study, other 3D-printing materials shall be tested to mimic real-surgical scenarios. This will include an in-depth characterisation of different cutting areas on the mandible and their resulting error and angular precision. Future work would also test the application on different HMDs than the HoloLens 2. Whether surgical-specific (such as the VOSTARS or the Xvision Spine System) or VST HMDs such as the Varjo XR-4 or the Apple Vision Pro, this would potentially enhance the accuracy and resolution of the application, thereby improving the precision of the system. As the real world is captured by cameras in VST HMDs, they are less dependent on ambient light conditions compared to OST HMDs, which rely on direct viewing of the physical environment (Badiali et al., 2020). The main challenge with the current HMDs used for surgical guidance is the accuracy of registration. While widely preferred in surgical applications due to their accessibility and low cost, HMDs such as the HoloLens are designed for general-purpose applications and are substandard for certain operations that require acute precision (Chegini et al., 2023). Moreover, visual discomfort, eye fatigue or migraines might be felt after prolonged use (Shibata et al., 2011). New "surgery-specific" HMDs in development will focus on improving main requirements such as reliability, safety and ergonomics (Qian et al., 2017). More precisely, characteristics such as low weight, ease of use, minimum calibration process, submillimetric registration accuracy with adequate image-object contrasts, and the integration of surgical instrument recognition algorithms are to be accounted for (Hussain et al., 2020). A registration time of 5 to 10 minutes and a tracking accuracy of 1 to 2 mm are reported to be acceptable scopes in maxillofacial surgery (Chu et al., 2017). Safety mechanisms ensuring the vision preservation of the surgical field in case of eventual software fault also need to be implemented (Liu et al., 2018).

Then, to establish the efficacy and safety of this AR-guided application, rigorous clinical testing is imperative. This will first include further in-vitro studies involving experienced and beginner surgeons in surgery-like conditions, implementing blood occlusion, time constraints or real surgical saw cutting. A direct measured comparison between the VSP and the AR method will then be performed. The most optimal viewing angle for initiating the registration shall also be studied and characterised.

Future work will investigate the extendibility of this framework with the fibula bone. Deformable tissues will also be investigated as potential models for the application. Furthermore, artificial

intelligence (AI) algorithms could assist in creating optimal surgical paths or training models to be optimally recognised, leading to better registration accuracy.

Following these tests, in-vivo accuracy assessments could be performed. These studies will aim to not only assess the immediate surgical outcomes but also track long-term patient and surgeon satisfaction. Such comprehensive data will be crucial for the wider acceptance and implementation of this application in clinical settings. It will then be important to address the ethical considerations. This includes ensuring patient consent for the use of AR, addressing data security concerns, and complying with medical regulatory standards. Future research must also consider the ethical implications of AI and machine learning decisions in surgical planning and execution.

Finally, while this work focused on mandible cutting aimed at maxillofacial surgery, it could be extended to other surgical applications. Indeed, the mandible Model Target presented in figure 3.6 can easily be replaced by another body anatomy. Similarly, the virtual content can be adapted to specific applications, guiding surgeons in other surgical contexts. For example, Percutaneous Nephrolithotomy (PCNL) is an operation that involves making a small incision in the patient's back and creating a tract directly into the kidney. Through this, the surgeon can insert instruments to break up and remove kidney stones (Häcker and Michel, 2019). According to Prof. Dr. Ben Van Cleynenbreugel (UZ, Leuven), while having a high success rate for experienced surgeons, young surgeons are more prone to errors due to limited intra-patient visibility, currently only accessed through real-time fluoroscopy. The proposed framework could provide further guidance in this operation, by displaying crucial virtual information, possibly improving the accuracy of the procedure.

6 CONCLUSION

This thesis presents a markerless augmented reality spatial guidance system for maxillofacial surgery. This approach addresses the longstanding challenge of transposing 2D images into 3D mental representations for accurate surgical navigation. Existing literature outlines the limitations of traditional methods in maxillofacial surgery, particularly the use of custom-made cutting guides. While these guides offer a precision of around 2 mm, they are cost-intensive, time-consuming, and invasive, thereby posing health risks to patients.

The introduction of VR, AR, and MR into medical fields has offered new perspectives for innovation in surgical procedures, enhancing both efficiency and precision. In particular, AR has emerged as a powerful tool in surgery, offering an immersive experience by overlaying digital information onto the real world, allowing surgeons to interact with both simultaneously. The synergy between real and virtual worlds is crucial for complex surgeries, like in maxillofacial interventions where dexterity and precision are paramount due to the proximity of nerves and vessels. This thesis builds upon these findings, proposing an AR-based solution that eliminates the need for physical cutting guides and reduces the invasiveness of surgical procedures. Materials and methods employed in this research involved the development and testing of the AR guidance system. This system enhances the surgeon's view by providing a real-time, virtual representation of planned mandible osteotomy trajectories. The proposed framework features a markerless tracking and registration technology, which relies on the patient's natural anatomical features. This approach not only reduces the invasiveness of the procedure but also adapts seamlessly to changes in surgical conditions, eliminating the need for positioning physical markers.

The main results from the in-vitro user study involving four surgeons were highly promising. The system demonstrated remarkable accuracy, with a hologram registration error of only 1.08 mm. An intra- and inter-operator accuracy assessment showed a mean registration error of less than 1.37 mm. These results highlight the system's potential to enhance the precision and efficiency of surgical procedures. The proposed AR system represents a major step forward in surgical practices. It offers a less invasive, more accurate, and time-efficient alternative to the traditional state-of-the-art methods. Furthermore, this system has the potential to significantly reduce the costs associated with surgical procedures, benefiting both healthcare providers and patients. This thesis not only addresses a critical gap in the current surgical practices but also sets a new standard in the use of AR technology in medical procedures. It opens new avenues for further research and development in the field of reconstructive surgery, potentially revolutionising surgical methodologies in the years to come.

BIBLIOGRAPHY

Ahn, J., Choi, H., Hong, J., and Hong, J. (2019). Tracking accuracy of a stereo camera-based augmented reality navigation system for orthognathic surgery. *Journal of Oral and Maxillofacial Surgery*, 77(5):1070–1070.

Badiali, G., Cercenelli, L., Battaglia, S., Marcelli, E., Marchetti, C., Ferrari, V., and Cutolo, F. (2020). Review on augmented reality in oral and cranio-maxillofacial surgery: Toward surgery-specific head-up displays. *IEEE Access*, 8:59015–59028.

Battaglia, S., Ricotta, F., Maiolo, V., Savastio, G., Contedini, F., Cipriani, R., Bortolani, B., Cercenelli, L., Marcelli, E., Marchetti, C., and Tarsitano, A. (2019). Computer-assisted surgery for reconstruction of complex mandibular defects using osteomyocutaneous microvascular fibular free flaps: Use of a skin paddle-outlining guide for soft-tissue reconstruction. a technical report. *Journal of Cranio-Maxillofacial Surgery*, 47(2):293–299.

Breeland, G., Aktar, A., and C. Patel, B. (2023). Anatomy, Head and Neck, Mandible - PubMed — pubmed.ncbi.nlm.nih.gov. `https://pubmed.ncbi.nlm.nih.gov/30335325/`. [Accessed 19-11-2023].

Brown, J., Lowe, D., Kanatas, A., and Schache, A. (2017). Mandibular reconstruction with vascularised bone flaps: a systematic review over 25 years. *British Journal of Oral and Maxillofacial Surgery*, 55(2):113–126.

Byers, J., Bittner, A., and Hill, S. (1989). *Advances in Industrial Ergonomics and Safety*, chapter Proceedings of the Annual International Industrial Ergonomics and Safety Conference Held in Cincinnati, Ohio, U.S.A., 5-9 June 1989, the Official Conference of the International Foundation for Industrial Ergonomics and Safety Research, Volume 1, pages 481–485. Taylor & Francis.

Casari, F. A., Navab, N., Hruby, L. A., Kriechling, P., Nakamura, R., Tori, R., de Lourdes dos Santos Nunes, F., Queiroz, M. C., Fürnstahl, P., and Farshad, M. (2021). Augmented reality in orthopedic surgery is emerging from proof of concept towards clinical studies: a literature review explaining the technology and current state of the art. *Current Reviews in Musculoskeletal Medicine*, 14(2):192–203.

Ceccariglia, F., Cercenelli, L., Badiali, G., Marcelli, E., and Tarsitano, A. (2022). Application of augmented reality to maxillary resections: A three-dimensional approach to maxillofacial oncologic surgery. *Journal of Personalized Medicine*, 12(12):2047.

Cercenelli, L., Babini, F., Badiali, G., Battaglia, S., Tarsitano, A., Marchetti, C., and Marcelli, E. (2022). Augmented reality to assist skin paddle harvesting in osteomyocutaneous fibular flap reconstructive surgery: A pilot evaluation on a 3d-printed leg phantom. *Frontiers in Oncology*, 11.

Chegini, S., Edwards, E., McGurk, M., Clarkson, M., and Schilling, C. (2023). Systematic review of techniques used to validate the registration of augmented-reality images using a head-mounted device to navigate surgery. *British Journal of Oral and Maxillofacial Surgery*, 61(1):19–27.

Chu, Y., Yang, J., Ma, S., Ai, D., Li, W., Song, H., Li, L., Chen, D., Chen, L., and Wang, Y. (2017). Registration and fusion quantification of augmented reality based nasal endoscopic surgery. *Medical Image Analysis*, 42:241–256.

Cleveland (2022). Osteotomy (Bone Cutting): What It Is, Procedure & Recovery — my.clevelandclinic.org. `https://my.clevelandclinic.org/health/articles/22688-osteotomy`. [Accessed 16-11-2023].

Condino, S., Turini, G., Parchi, P. D., Viglialoro, R. M., Piolanti, N., Gesi, M., Ferrari, M., and Ferrari, V. (2018). How to build a patient-specific hybrid simulator for orthopaedic open surgery: Benefits and limits of mixed-reality using the microsoft HoloLens. *Journal of Healthcare Engineering*, 2018:1–12.

De Ketele, A., Meeus, J., Shaheen, E., Verstraete, L., and Politis, C. (2023). The usefulness of cutting guides for resection or biopsy of mandibular lesions: A technical note and case report. *Journal of Stomatology, Oral and Maxillofacial Surgery*, 124(1):101272.

Dewitz, B., Bibo, R., Moazemi, S., Kalkhoff, S., Recker, S., Liebrecht, A., Lichtenberg, A., Geiger, C., Steinicke, F., Aubin, H., and Schmid, F. (2022). Real-time 3d scans of cardiac surgery using a single optical-see-through head-mounted display in a mobile setup. *Frontiers in Virtual Reality*, 3.

Dong, S., Du, C., He, B., Zhu, Z., Han, D., Jin, W., Lin, H., and Shi, B. (2023). Application of an effective markerless augmented reality image guidance method in dental implant surgery. *The International Journal of Medical Robotics and Computer Assisted Surgery*, 19(4):2523.

Dong, Z., Li, B., Xie, R., Wu, Q., Zhang, L., and Bai, S. (2017). Comparative study of three kinds of fibula cutting guides in reshaping fibula for the reconstruction of mandible: An accuracy simulation study in-vitro. *Journal of Cranio-Maxillofacial Surgery*, 45(8):1227–1235.

Eckardt, C. and Paulo, E. B. (2016). Heads-up surgery for vitreoretinal procedures: An experimental and clinical study. *Retina*, 36(1):137–147.

Estrada, J., Paheding, S., Yang, X., and Niyaz, Q. (2022). Deep-learning-incorporated augmented reality application for engineering lab training. *Applied Sciences*, 12(10):5159.

Frantz, T., Jansen, B., Duerinck, J., and Vandemeulebroucke, J. (2018). Augmenting microsoft's HoloLens with vuforia tracking for neuronavigation. *Healthcare Technology Letters*, 5(5):221–225.

Goormans, F., Sun, Y., Bila, M., Schoenaers, J., Geusens, J., Lübbers, H.-T., Coucke, W., and Politis, C. (2019). Accuracy of computer-assisted mandibular reconstructions with free fibula flap: Results of a single-center series. *Oral Oncology*, 97:69–75.

Häcker, A. and Michel, M. (2019). Perkutane nephrolitholapaxie (pcnl). *Aktuelle Urologie*, 50(02):203–212.

Hussain, R., Lalande, A., Guigou, C., and Bozorg-Grayeli, A. (2020). Contribution of augmented reality to minimally invasive computer-assisted cranial base surgery. *IEEE Journal of Biomedical and Health Informatics*, 24(7):2093–2106.

Incekara, F., Smits, M., Dirven, C., and Vincent, A. (2018). Clinical feasibility of a wearable mixed-reality device in neurosurgery. *World Neurosurgery*, 118:422–427.

Kavitha, A., Kumar, S. P., Darsana, G., and Sudhir, G. (2023). Enhancing visualization of surgical tool through integrated motion tracking system. In *Extended Reality*, pages 395–404. Springer Nature Switzerland.

Ke, S., Xiang, F., Zhang, Z., and Zuo, Y. (2019). A enhanced interaction framework based on vr, ar and mr in digital twin. *Procedia CIRP*, 83:753–758.

Kim, Y. C., Lee, S. J., Park, C.-U., Jeong, W. S., Na, S. W., and Choi, J. W. (2023). Application of augmented reality using automatic markerless registration for facial plastic and reconstructive surgery. *Journal of Cranio-Maxillofacial Surgery*.

Kunz, C., Maurer, P., Kees, F., Henrich, P., Marzi, C., Hlaváč, M., Schneider, M., and Mathis-Ullrich, F. (2020). Infrared marker tracking with the HoloLens for neurosurgical interventions. *Current Directions in Biomedical Engineering*, 6(1).

Lee, D., Yi, J. W., Hong, J., Chai, Y. J., Kim, H. C., and Kong, H.-J. (2018). Augmented reality to localize individual organ in surgical procedure. *Healthcare Informatics Research*, 24(4):394.

Liebmann, F., Roner, S., von Atzigen, M., Scaramuzza, D., Sutter, R., Snedeker, J., Farshad, M., and Fürnstahl, P. (2019). Pedicle screw navigation using surface digitization on the microsoft HoloLens. *International Journal of Computer Assisted Radiology and Surgery*, 14(7):1157–1165.

Liu, H., Auvinet, E., Giles, J., and Rodriguez y Baena, F. (2018). Augmented reality based navigation for computer assisted hip resurfacing: A proof of concept study. *Annals of Biomedical Engineering*, 46(10):1595–1605.

Liu, H. and Baena, F. R. Y. (2020). Automatic markerless registration and tracking of the bone for computer-assisted orthopaedic surgery. *IEEE Access*, 8:42010–42020.

Mai, H.-N., Dam, V. V., and Lee, D.-H. (2023). Accuracy of augmented reality-assisted navigation in dental implant surgery: Systematic review and meta-analysis. *Journal of Medical Internet Research*, 25:42040.

Martin-Gomez, A., Li, H., Song, T., Yang, S., Wang, G., Ding, H., Navab, N., Zhao, Z., and Armand, M. (2022). Sttar: Surgical tool tracking using off-the-shelf augmented reality head-mounted displays. `https://arxiv.org/abs/2208.08880`. [Online; accessed October 14, 2023].

McCloskey, K., Turlip, R., Ahmad, H. S., Ghenbot, Y. G., Chauhan, D., and Yoon, J. W. (2023). Virtual and augmented reality in spine surgery: A systematic review. *World Neurosurgery*, 173:96–107.

MedlinePlus (2020). Anastomosis: MedlinePlus Medical Encyclopedia — medlineplus.gov. `https://medlineplus.gov/ency/article/002231.htm`. [Accessed 16-11-2023].

Microsoft (2023a). Documentation du developpeur MRTK2-Unity - MRTK 2. https://learn.microsoft.com/fr-fr/windows/mixed-reality/mrtk-unity/mrtk2/?view=mrtkunity-2022-05. [Accessed 11-11-2023].

Microsoft (2023b). Microsoft HoloLens — Mixed Reality Technology for Business. https://www.microsoft.com/en-us/hololens. [Accessed 30-12-2023].

Mischkowski, R. A., Zinser, M. J., Kübler, A. C., Krug, B., Seifert, U., and Zöller, J. E. (2006). Application of an augmented reality tool for maxillary positioning in orthognathic surgery – a feasibility study. *Journal of Cranio-Maxillofacial Surgery*, 34(8):478–483.

NASA (2020). Nasa tlx task load index. https://humansystems.arc.nasa.gov/groups/tlx/index.php. [Accessed 29-11-2023].

Palumbo, M. C., Morchi, L., Corbetta, V., Menciassi, A., De Momi, E., Votta, E., and Redaelli, A. (2022). An easy and user independent augmented reality based navigation system for radiation-free interventional procedure. In *2022 International Symposium on Medical Robotics (ISMR)*. IEEE.

Patel, S. Y., Kim, D. D., and Ghali, G. E. (2019). Maxillofacial reconstruction using vascularized fibula free flaps and endosseous implants. *Oral and Maxillofacial Surgery Clinics of North America*, 31(2):259–284.

Pepe, A., Trotta, G. F., Mohr-Ziak, P., Gsaxner, C., Wallner, J., Bevilacqua, V., and Egger, J. (2019). A marker-less registration approach for mixed reality-aided maxillofacial surgery: a pilot evaluation. *Journal of Digital Imaging*, 32(6):1008–1018.

Pham Dang, N., Chandelon, K., Barthelemy, I., Devoize, L., and Bartoli, A. (2021). A proof-of-concept augmented reality system in oral and maxillofacial surgery. *Journal of Stomatology, Oral and Maxillofacial Surgery*, 122(4):338–342.

Pietruski, P., Majak, M., Swiatek-Najwer, E., Zuk, M., Popek, M., Jaworowski, J., and Mazurek, M. (2019). Supporting fibula free flap harvest with augmented reality: A proof-of-concept study. *The Laryngoscope*, 130(5):1173–1179.

Piramide, C., Ulrich, L., Piazzolla, P., and Vezzetti, E. (2022). Toward supporting maxillo-facial surgical guides positioning with mixed reality—a preliminary study. *Applied Sciences*, 12(16):8154.

PTC (2023). Vuforia, market-leading enterprise ar. https://www.ptc.com/en/products/vuforia. [Accessed 17-11-2023].

Qian, L., Barthel, A., Johnson, A., Osgood, G., Kazanzides, P., Navab, N., and Fuerst, B. (2017). Comparison of optical see-through head-mounted displays for surgical interventions with object-anchored 2d-display. *International Journal of Computer Assisted Radiology and Surgery*, 12(6):901–910.

Sadeghi-Niaraki, A. and Choi, S.-M. (2020). A survey of marker-less tracking and registration techniques for health &amp environmental applications to augmented reality and ubiquitous geospatial information systems. *Sensors*, 20(10):2997.

Scolozzi, P. and Bijlenga, P. (2017). Removal of recurrent intraorbital tumour using a system of augmented reality. *British Journal of Oral and Maxillofacial Surgery*, 55(9):962–964.

Shibata, T., Kim, J., Hoffman, D. M., and Banks, M. S. (2011). The zone of comfort: Predicting visual discomfort with stereo displays. *Journal of Vision*, 11(8):11–12.

Spirig, J. M., Roner, S., Liebmann, F., Fürnstahl, P., and Farshad, M. (2021). Augmented reality-navigated pedicle screw placement: a cadaveric pilot study. *European Spine Journal*, 30(12):3731–3737.

Stucki, J., Dastgir, R., Baur, D. A., and Quereshy, F. A. (2023). The use of virtual reality and augmented reality in oral and maxillofacial surgery: A narrative review. *Oral Surgery, Oral Medicine, Oral Pathology and Oral Radiology*.

Succo, G., Berrone, M., Battiston, B., Tos, P., Goia, F., Appendino, P., and Crosetti, E. (2014). Step-by-step surgical technique for mandibular reconstruction with fibular free flap: application of digital technology in virtual surgical planning. *European Archives of Oto-Rhino-Laryngology*, 272(6):1491–1501.

Suenaga, H., Tran, H. H., Liao, H., Masamune, K., Dohi, T., Hoshi, K., and Takato, T. (2015). Vision-based markerless registration using stereo vision and an augmented reality surgical navigation system: a pilot study. *BMC Medical Imaging*, 15(1).

Tarsitano, A., Mazzoni, S., Cipriani, R., Scotti, R., Marchetti, C., and Ciocca, L. (2014). The cad-cam technique for mandibular reconstruction: An 18 patients oncological case-series. *Journal of Cranio-Maxillofacial Surgery*, 42(7):1460–1464.

Tremosa, L. (2023). Beyond ar vs. vr: What is the difference between ar vs mr vs vr vs xr? interaction design foundation. https://www.interaction-design.org/literature/article/beyond-ar-vs-vr-what-is-the-difference-between-ar-vs-mr-vs-vr-vs-xr. [Accessed 29-12-2023].

Trotta, G. F., Pellicciari, R., Boccaccio, A., Brunetti, A., Cascarano, G. D., Manghisi, V. M., Fiorentino, M., Uva, A. E., Defazio, G., and Bevilacqua, V. (2019). A neural network-based software to recognise blepharospasm symptoms and to measure eye closure time. *Computers in Biology and Medicine*, 112:103376.

Unity (2023). Plateforme de developpement en temps reel Unity — Moteur 3D, 2D, RV et RA. https://unity.com/fr. [Accessed 11-11-2023].

Verhey, J. T., Haglin, J. M., Verhey, E. M., and Hartigan, D. E. (2020). Virtual, augmented, and mixed reality applications in orthopedic surgery. *The International Journal of Medical Robotics and Computer Assisted Surgery*, 16(2).

Vuforia (2023). Vuforia Engine Overview — Vuforia Library. https://developer.vuforia.com/library/getting-started/vuforia-features. [Accessed 17-11-2023].

VuforiaMTG (2023). Advanced Model Target Databases — Vuforia Library — developer.vuforia.com. https://developer.vuforia.com/library/model-targets/advanced-model-target-databases. [Accessed 19-11-2023].

Wang, J., Shen, Y., and Yang, S. (2019). A practical marker-less image registration method for augmented reality oral and maxillofacial surgery. *International Journal of Computer Assisted Radiology and Surgery*, 14(5):763–773.

Wang, J., Suenaga, H., Hoshi, K., Yang, L., Kobayashi, E., Sakuma, I., and Liao, H. (2014). Augmented reality navigation with automatic marker-free image registration using 3-d image overlay for dental surgery. *IEEE Transactions on Biomedical Engineering*, 61(4):1295–1304.

Wijbenga, J. G., Schepers, R. H., Werker, P. M., Witjes, M. J., and Dijkstra, P. U. (2016). A systematic review of functional outcome and quality of life following reconstruction of maxillofacial defects using vascularized free fibula flaps and dental rehabilitation reveals poor data quality. *Journal of Plastic, Reconstructive amp; Aesthetic Surgery*, 69(8):1024–1036.

Wybaillie, G. (2022). Developments towards an augmented reality application for maxillofacial surgery. Master's thesis, Katholieke Universiteit Leuven (KUL), Leuven, Belgium. Unpublished master's thesis.

Yadav, N. (2018). Understanding display techniques in Augmented Reality. `https://blog.prototypr.io/understanding-display-techniques-in-augmented-reality`. [Accessed 31-12-2023].

Zhu, M., Liu, F., Chai, G., Pan, J. J., Jiang, T., Lin, L., Xin, Y., Zhang, Y., and Li, Q. (2017). A novel augmented reality system for displaying inferior alveolar nerve bundles in maxillofacial surgery. *Scientific Reports*, 7(1).

Zinser, M. J., Mischkowski, R. A., Dreiseidler, T., Thamm, O. C., Rothamel, D., and Zöller, J. E. (2013). Computer-assisted orthognathic surgery: waferless maxillary positioning, versatility, and accuracy of an image-guided visualisation display. *British Journal of Oral and Maxillofacial Surgery*, 51(8):827–833.

APPENDICES

A Python code for the EM sensor point cloud acquisition A-1

B NASA Task Load Index and questionnaire results B-4

APPENDIX A : PYTHON CODE FOR THE EM SENSOR POINT CLOUD ACQUISITION

Python code for the EM sensor point cloud acquisition

```
import numpy as np
from sksurgerynditracker.nditracker import NDITracker
import msvcrt
import time
from matplotlib import pyplot as plt



 # Points in {EM}
p0EM = None
p1EM = None

# creating empty lists for the points
pGuides = []
pHololens = []

######################
# Start EM tracking #
######################
# add a folder named rom where there are the rom files
SETTINGS = {
            "tracker type": "aurora",
            "romfiles" : ["../rom/Thin_6DOF_610060.rom","../rom
                ↪ /610058-5DOF.rom"],
            # "ports to probe" : 1
                }
TRACKER = NDITracker(SETTINGS)

TRACKER.start_tracking()
TRACKER.use_quaternions = True

print('Register the points in EM frame by pressing 0, 1. Then press
    ↪  Q to save and exit...')
while True:
    a = time.time()
    port_handles, timestamps, framenumbers, tracking, quality =
        ↪ TRACKER.get_frame()
    t = tracking[0]
    t = np.where(np.isnan(t), 0, t)
    q0 = t[0][0]
    qx = t[0][1]
    qy = t[0][2]
    qz = t[0][3]
    tx = t[0][4]
    ty = t[0][5]
    tz = t[0][6]
```

```
44
45
46      tEM = np.array([tx,ty,tz, qx,qy,qz,q0])
47
48      if  msvcrt.kbhit(): # handle keyboard hits if available
49          k = msvcrt.getch()
50          a = k.decode('ascii')
51
52          if a == '0':
53              p0EM = tEM
54              print('P0 saved: ', p0EM)
55
56              # Add point to the list
57              pGuides.append(tEM)
58
59          if a == '1':
60              p1EM = tEM
61              print('P1 saved: ', p1EM)
62
63              # Add point to the list
64              pHololens.append(tEM)
65
66
67          if a == 'q':
68              print('Quitting, calculating transformation matrix')
69              break
70
71
72
73  # Save points row by row
74  # np.savetxt('points.csv',np.array([p0EM,p1EM,p2EM,p3EM]))
75  # save the array also with points row by row, after converting the
        ↪ list to np array
76  pGuides = np.asarray(pGuides)
77  pHololens = np.asarray(pHololens)
78  np.savetxt('M31_pointArrays.csv',pGuides)
79  np.savetxt('M31_pointArraysHolo.csv',pHololens)
80
81  # can also calculate the errors between the consecutive points, or
        ↪ also just along x and y...
82  error = np.sqrt(np.power(pGuides[:,0]-pHololens[:,0],2)+ np.power(
        ↪ pGuides[:,1]-pHololens[:,1],2)+np.power(pGuides[:,2]-
        ↪ pHololens[:,2],2))
83  # plot results
84  #print(error)
85  np.savetxt('M31_Error.csv',error)
86  fig = plt.figure()
87  ax = fig.add_subplot(projection='3d')
88
89
90  # plot whole array
91  ax.scatter(pGuides[:,0],pGuides[:,1],pGuides[:,2])
92  ax.scatter(pHololens[:,0],pHololens[:,1],pHololens[:,2])
```

```
# plot errors
figError = plt.figure()
plt.plot(error)
plt.show()

TRACKER.stop_tracking()
TRACKER.close()
print('Exiting...')
```

Python code to calculate a mean value inside any given .csv file

```
import csv

# Specify the path to your CSV file
csv_file_path = 'M34_Error.csv'

# Specify the column index (assuming it's the first column, change accordingly)
column_index = 0

# Read the CSV file and extract the values from the specified column
values = []
with open(csv_file_path, 'r') as file:
    reader = csv.reader(file)
    for row in reader:
        try:
            value = float(row[column_index])
            values.append(value)
        except (ValueError, IndexError):
            # Handle cases where the value cannot be converted to float or index is out of range
            pass

# Calculate the mean
if values:
    mean_value = sum(values) / len(values)
    print(f'The mean of the values in the specified column is: {mean_value}')
else:
    print('No valid values found in the specified column.')
```

APPENDIX B : NASA TASK LOAD INDEX AND QUESTIONNAIRE RESULTS

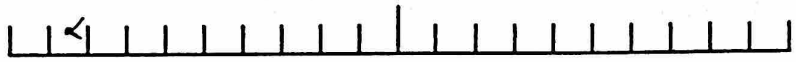
Name: W DE VOS N°: 1 Date: 28/11/23

NASA Task Load Index (TLX) (Page 1/2)

In order to assess the workload you experienced while completing the task, we ask you to rate several factors individually on the scales provided below.

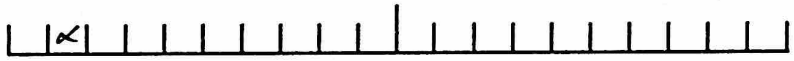
Note: Performance goes from good (left) to bad (right)

Mental Demand — How mentally demanding was the task?



Very Low — Very High

Physical Demand — How physically demanding was the task?



Very Low — Very High

Temporal Demand — How hurried or rushed was the pace of the task?



Very Low — Very High

Performance — How successful were you in accomplishing what you were asked to do?



Perfect — Failure

Effort — How hard did you have to work to accomplish your level of performance?



Very Low — Very High

Frustration — How insecure, discouraged, irritated, stressed, and annoyed wereyou?



Very Low — Very High

Créé avec Tiny Scanner

Questionnaire on the usability of the system (Page 2/2)

1. Is there anything you liked during the experiment?

- perceived accuracy (subjective)
- novelty

2. Is there anything you are not satisfied with or did not like during the experiment?

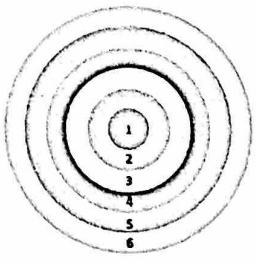
- stability of software
- absence of opacity setting
- FDM print texture lines (layer lines)

3. What suggestions do you have to improve the system?

- opacity slider
- resin prints

DO NOT FILL THIS PART

	SPHERES TEST - HOLOGRAM ACCURACY ASSESSMENT
Front View	RED
Side View	RED
Top View	RED



	Mandible 1	Mandible 2	Mandible 3	Cutting Guides
Time taken for drawing the 4 osteotomy lines	4:13	2:15	2:11	1:31

Créé avec Tiny Scanner

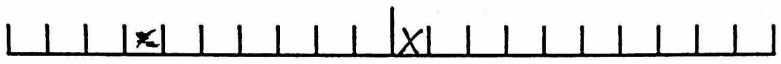
Name: Fedoua Madadi N°: 2 Date:

NASA Task Load Index (TLX) (Page 1/2)

In order to assess the workload you experienced while completing the task, we ask you to rate several factors individually on the scales provided below.

Note: Performance goes from good (left) to bad (right)

Mental Demand — How mentally demanding was the task?



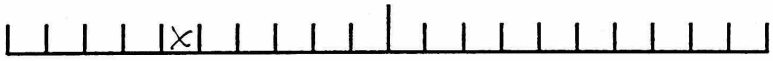
Very Low — Very High

Physical Demand — How physically demanding was the task?



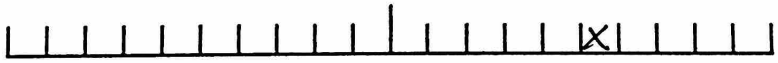
Very Low — Very High

Temporal Demand — How hurried or rushed was the pace of the task?



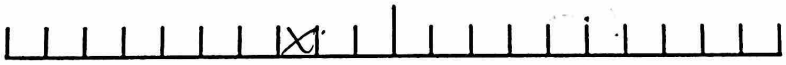
Very Low — Very High

Performance — How successful were you in accomplishing what you were asked to do?



Perfect — Failure

Effort — How hard did you have to work to accomplish your level of performance?



Very Low — Very High

Frustration — How insecure, discouraged, irritated, stressed, and annoyed wereyou?



Very Low — Very High

Créé avec Tiny Scanner

Questionnaire on the usability of the system (Page 2/2)

1. Is there anything you liked during the experiment?

Yes! Very educational.

2. Is there anything you are not satisfied with or did not like during the experiment?

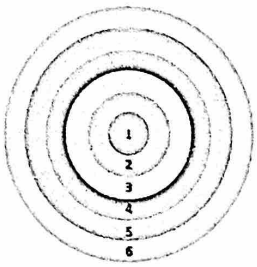
- the overlay of the virtual and fysical model did not match entirely, this made the tactile dept estimation difficult.
- during movement of the fysical model a delay of a second until the digital model overlays

3. What suggestions do you have to improve the system?

- Improve the time delays, because movements of the model cause deviations in ~~de~~ the cutting line
- More exact overlay

DO NOT FILL THIS PART

	SPHERES TEST - HOLOGRAM ACCURACY ASSESSMENT
Front View	RED
Side View	RED
Top View	BLUE



	Mandible 1	Mandible 2	Mandible 3	Cutting Guides
Time taken for drawing the 4 osteotomy lines	3:51	3:15	1:03	

Créé avec Tiny Scanner

(RH)

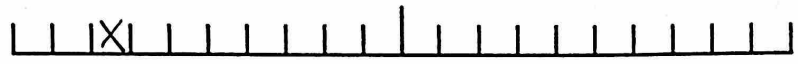
Name: VR VERCRUYSSE **N°:** 3 **Date:**

NASA Task Load Index (TLX) (Page 1/2)

In order to assess the workload you experienced while completing the task, we ask you to rate several factors individually on the scales provided below.

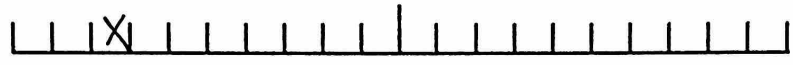
Note: Performance goes from good (left) to bad (right)

Mental Demand How mentally demanding was the task?



Very Low Very High

Physical Demand How physically demanding was the task?



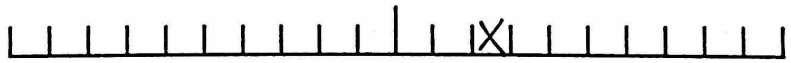
Very Low Very High

Temporal Demand How hurried or rushed was the pace of the task?



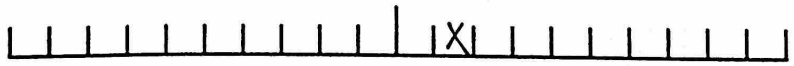
Very Low Very High

Performance How successful were you in accomplishing what you were asked to do?



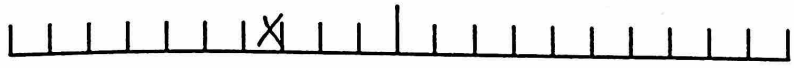
Perfect Failure

Effort How hard did you have to work to accomplish your level of performance?



Very Low Very High

Frustration How insecure, discouraged, irritated, stressed, and annoyed wereyou?



Very Low Very High

Créé avec Tiny Scanner

Questionnaire on the usability of the system (Page 2/2)

1. Is there anything you liked during the experiment?

Great potential

2. Is there anything you are not satisfied with or did not like during the experiment?

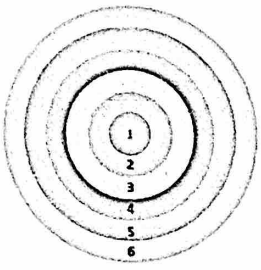
- Change plane to a line as plane blocks the view

3. What suggestions do you have to improve the system?

See above

DO NOT FILL THIS PART

	SPHERES TEST - HOLOGRAM ACCURACY ASSESSMENT
Front View	RED
Side View	RED
Top View	RED



	Mandible 1	Mandible 2	Mandible 3	Cutting Guides
Time taken for drawing the 4 osteotomy lines	2:57	2:45	2:15	1:05

Créé avec Tiny Scanner

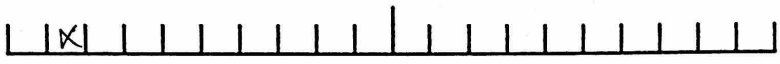
Name: MAXIME PEETERS **N°:** 4 **Date:**

NASA Task Load Index (TLX) (Page 1/2)

In order to assess the workload you experienced while completing the task, we ask you to rate several factors individually on the scales provided below.

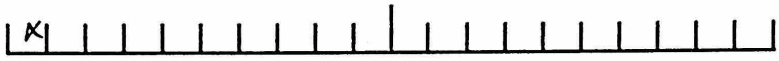
Note: Performance goes from good (left) to bad (right)

Mental Demand — How mentally demanding was the task?



Very Low — Very High

Physical Demand — How physically demanding was the task?



Very Low — Very High

Temporal Demand — How hurried or rushed was the pace of the task?



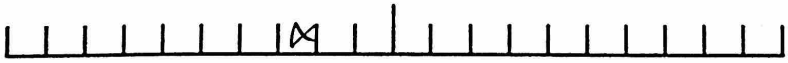
Very Low — Very High

Performance — How successful were you in accomplishing what you were asked to do?



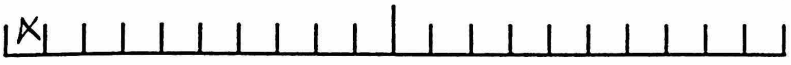
Perfect — Failure

Effort — How hard did you have to work to accomplish your level of performance?



Very Low — Very High

Frustration — How insecure, discouraged, irritated, stressed, and annoyed wereyou?



Very Low — Very High

Créé avec Tiny Scanner

Questionnaire on the usability of the system (Page 2/2)

1. Is there anything you liked during the experiment?

Astonishing how accurate (never used VR / Augmented reality before)

2. Is there anything you are not satisfied with or did not like during the experiment?

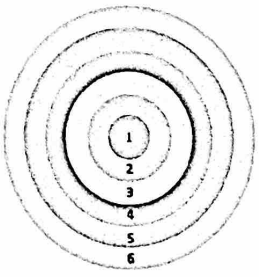
Sometimes the cutting planes were really blurry.

3. What suggestions do you have to improve the system?

Higher resolution of cutting planes.

DO NOT FILL THIS PART

	SPHERES TEST - HOLOGRAM ACCURACY ASSESSMENT
Front View	BLUE
Side View	BLUE
Top View	BLUE



	Mandible 1	Mandible 2	Mandible 3	Cutting Guides
Time taken for drawing the 4 osteotomy lines	4:50	1:15	1:35	1:27

Créé avec Tiny Scanner

FACULTY OF ENGINEERING TECHNOLOGY
CAMPUS GROUP T LEUVEN
Andreas Vesaliusstraat 13
3000 LEUVEN, Belgium
tel. +32 16 30 10 30
fax +32 16 30 10 40
fet.groupt@kuleuven.be
www.iiw.kuleuven.be